Monitoring large populations of locus coeruleus neurons reveals the non-global nature of the norepinephrine neuromodulatory system

Nelson K. Totah[1], Ricardo M. Neves[1], Stefano Panzeri[2], Nikos K. Logothetis[1,3], Oxana Eschenko[1]

[1]Dept. of Physiology of Cognitive Processes, Max Planck Institute for Biological Cybernetics, Spemannstrasse 38, 72076, Tuebingen, Germany

[2]Laboratory of Neural Computation, Istituto Italiano di Tecnologia, Corso Bettini 31, 38068, Rovereto, Italy

[3]Div. Of Imaging Science and Biomedical Engineering, University of Manschester, M13 9PT Manchester, United Kingdom

Correspondence and requests should be addressed to Dr. Nelson Totah (nelson.totah@tuebingen.mpg.de), Dr. Oxana Eschenko (oxana.eschenko@tuebingen.mpg.de)

Abstract

The non-specific neuromodulation of the forebrain by the noradrenergic locus coeruleus (LC) is a foundation of wide-ranging theories of cognitive and systems neuroscience. The non-specificity is assumed because of the diffuse projections of the nucleus as well as the synchronous spiking of its neurons. Synchrony, however, has never been assessed in a large population of LC cells, i.e. single units, nor has it been systematically related to specificity of their projection targets. Here, we recorded up to 52 single units simultaneously (3164 unit pairs) in the rat LC, and characterized forebrain projection patterns using antidromic stimulation. Two novel unit types were characterized; they differed by waveform shape, firing rate, and propensity for synchronization. Cross-correlation analysis revealed a surprisingly poor correlation between unit spiking; only 13% of unit pairs had response profiles reflecting synchronization due to common synaptic input or gap junctions. While LC unit spikes were phase locked to cortical slow oscillations (< 2 Hz), they did so intermittently, yielding poor population synchronization. A novel infra-slow (0.01-1 Hz) spiking fluctuation was observed in LC units, yet this too was asynchronous across unit pairs. A highly synchronized minority had a stronger tendency for targeted forebrain neuromodulation. Our findings demonstrate that the LC may convey a more complex and differentiated neuromodulatory signal than is widely assumed.

Introduction

The noradrenergic nucleus locus coeruleus (LC) in the rat brainstem consists of merely ~1,600 norepinephrine (NE) neurons but, through diffuse forebrain projections, it regulates a multitude of brain functions, such as arousal, perception, decision-making, and memory (*1*). The predominant view is that LC is a non-specific neuromodulatory system: its neurons act synchronously to modulate many forebrain targets via simultaneous NE release (*2*-*6*). The seemingly undifferentiated activity of LC has influenced diverse theories ranging from neural control of sleep to computational models of decision making (*2*, *7*-*10*). This perspective of LC function emerged primarily from two lines of research. The first one comprised anatomical and neurochemical studies demonstrating that the axons of individual LC neurons branch widely to innervate distant forebrain regions where their terminals can release NE, spreading up to ~100 μm from each active site (*11*-*14*). The second line included electrophysiological experiments showing that, in LC, multi-unit activity (MUA) is synchronized with changes in the local field potential (LFP, a marker of transmembrane currents and other peri-synaptic activity within LC), that were registered synchronously with spatially segregated electrodes placed in the core of the nucleus. (*6*, *15*, *16*). Thus, units throughout the nucleus are thought to respond in unison.

Although recent anatomical studies have demonstrated that individual LC neurons can target different cortical sites (*17*, *18*), synchronous activity across LC neurons would still result in global, non-specific forebrain neuromodulation. Indeed, electrical or optogenetic stimulation of the LC, which likely activates all LC neurons simultaneously, has been shown to evoke simultaneous NE release throughout multiple cortical sites and the cerebellum, hippocampus, and spinal cord (*19*, *20*). However, MUA does not necessarily provide an accurate estimate of synchrony because single units spiking independently, have been averaged over. Single unit recordings in LC, though, are rare due to technical challenges. Specifically, the small size of the LC has permitted mainly single wire recordings and the single unit waveforms of the densely packed LC cell bodies are difficult to isolate using a single recording channel. At present, only one study in the awake monkey and one study in the anesthetized rat have managed to simultaneously monitor two single units, and the reported findings were based on small data sets, e.g. ~20 pairs of neighboring single units recorded on the same electrode (*21*, *22*). Evidently under these

conditions it is impossible to infer the degree of synchronicity of the entire LC neuronal population.

To address this question, we recorded a large population of single units using a high-density recording array that covered the dorsal-ventral extent of LC in rats during urethane anesthesia (*23*, *24*). We could simultaneously monitor up to 52 single units and isolated 235 single units in 12 rats, yielding 3164 unit pairs. These data allowed us to examine, in unprecedented detail, synchrony among LC single units. In addition, we used forebrain electrical stimulation to evoke antidromic responses in LC units and assess whether correlated units projected to similar forebrain sites.

Here, we report the first evidence that synchrony in the LC is rare. Pairwise spike count correlations were close to zero and 87% of spike train cross-correlations revealed no significant synchrony. Although individual LC single units were phase locked to cortical LFP slow waves (< 2 Hz), multiple LC single units did not fire in synchrony on each cycle. We also observed novel rhythmic fluctuations in LC single unit firing rate on infra-slow timescales (<0.1 to 1 Hz), but these fluctuations too, were asynchronous across unit pairs. Only a minority (13% of unit pairs) were synchronized on the time scale of shared synaptic inputs (tens of milliseconds) or gap junctions (sub-millisecond). Antidromic responses of LC units revealed that synchronized units, coupled by putative gap junctions, were more likely to project to the same forebrain areas and, therefore, may provide targeted neuromodulation. We characterized two types of LC single units not previously described. Cell types differed by waveform shape, firing rate, propensity for synchronization, and relationship with cortical slow waves. Overall, the present findings suggest that LC activity is finely structured and is capable of targeted, in addition to non-specific, forebrain neuromodulation.

Results

Our objective was to characterize the degree of neuronal synchrony in the LC. Synchronous population activity would manifest as positive pairwise spike count correlations, regardless of the mechanism(s) underlying the synchrony. Specific mechanisms underlying synchronous spiking, such as common synaptic input or gap junctions, would appear in spike train cross-correlograms as broad (10's of msec) zero-centered peaks or sub-millisecond peaks,

respectively (*25-27*). Another potential mechanism for synchrony across LC neurons may involve interactions between cortex, thalamus, and LC that drive cortical slow wave oscillations. This mechanism would appear as entrainment of LC discharge to cortical oscillations that is synchronized across LC neurons (*28-30*). We quantified each of these measures of synchrony in the LC.

Identification and characterization of two distinct LC single unit types

We isolated 235 single units in 12 rats and recorded 5 to 52 individual LC units simultaneously (on average, ~20 units recorded simultaneously per rat; **Table 1**). Single units exhibited typical electrophysiological and pharmacological characteristics of LC units (see Supplementary Materials). The extracellular spike waveform shapes of LC single units separated into 2 types based on their spike width and after-hyperpolarization amplitude (**Figure 1A, B**). We will refer to these populations as “wide” and “narrow” units. Out of 235 single units, 34 units were narrow (14%) and 201 units were wide (86%). Interestingly, beyond distinct spike shape profile, these units had a number of characteristic differences: Narrow units discharged at significantly higher rates compared to wide units (1.34±0.13 spikes/sec and 0.81±0.05 spikes/sec, respectively; **Figure 1C, D)**. Both unit types were often recorded simultaneously, but narrow units were recorded in 7 out of 12 rats, possibly because of fewer units with narrow waveform reducing their probability of detection (**Table 1**). Both wide and narrow units responded to foot shocks (**Supplementary Figure 1**) and all units were inhibited by clonidine, suggesting that both unit types are noradrenergic (See Supplementary Materials on characterization of units). It is unlikely that the narrow units were local interneurons because stimulation of forebrain sites elicited antidromic responses in 30% of narrow units, thus confirming that narrow units are LC projection neurons.

We measured orthodromic responses of both unit types after stimulating either the prelimbic (PL) or infralimbic (IL) divisions of the prefrontal cortex (PFC). We observed both increases and decreases in spike rate (**Supplementary Figure 2**). The predominant response of LC units was to decrease spiking after PFC stimulation (35.1% for PL stimulation and 25.2% for IL stimulation); however, a small proportion of units (4.5% for PL stimulation and 8.1% for IL stimulation) increased their spike rate. The predominance of inhibition occurred for both unit types (**Figure 1E**). Strikingly, the different unit types responded to PFC stimulation with different latencies

(**Figure 1F**). Excitation occurred significantly earlier in wide units (90±21 msec for wide versus 440±162 msec for narrow; two-way t-test, T(60)=-4.16, p=0.0001), whereas inhibition occurred significantly earlier in narrow units (50±0 msec for wide versus 175±10 msec for narrow; T(187)=3.15, p=0.002). This result suggests differential and cell-type specific top-down regulation of LC activity.

LC single units have near-zero spontaneous and evoked spike count correlations

In order to quantify the magnitude and distribution of synchrony in the LC, we first quantified the discharge similarity between LC single units by calculating the Pearson correlation between the binned spike counts of unit pairs (N = 3164 pairs). The correlations coefficients were distributed around zero (**Figure 2A**). The mean correlation coefficient was 0.044±0.001 for 200 msec bins and 0.098±0.003 for 1 sec bins. Pairwise correlated variability was similar throughout the LC nucleus (**Supplementary Figure 3**).

Salient sensory stimuli are thought to drive the LC to burst synchronously (*16*). We applied a sensory stimulus (a single foot shock, 0.5 mA, 5.0 μsec pulse duration) and measured evoked spike count correlations in 2 time windows after stimulus onset (50 msec and 200 msec). The shorter window was chosen to focus on the initial transient burst of stimulus-evoked spikes. The longer window was chosen to compare the correlated activity evoked by the foot shock with correlations during spontaneous activity which were measured with a 200 msec window. The mean evoked spike count correlation was distributed around zero for both time windows (**Figure 2B, C**). Strikingly, a large number of negative spike count correlations emerged (**Figure 2B, C**). Spike count correlations during 200 msec after stimulus onset did not depend on distance between units (**Supplementary Figure 3**).

Although the entire population of LC units exhibited overall weak correlations, it is possible that different unit types could be synchronously active within each group of units. We assessed this possibility by examining the spontaneous and stimulus-evoked spike count correlations between pairs of the same type or mixed type. Pairs of narrow units exhibited higher correlations during spontaneous activity (**Figure 2D**) (ANOVA, pairwise unit type as factor; F(2,3163)=20.41, p=1.55E-9) in comparison to pairs of wide units (**Figure 2G**) (post-hoc t-test, p<0.0001) and pairs of mixed unit type (**Figure 2J**) (p<0.0001). The correlation coefficients were not significantly different depending on unit type for evoked activity (**Figure 2E**, **F**, **H**, **I**, **K**, **L**). Nevertheless, the

mean correlation for pairs of narrow units was still near zero, which suggests that the neither type of LC unit formed a highly correlated sub-population with other units of the same type. Remarkably, large numbers of negatively correlated pairs were observed only when the pair included a wide unit (**Figure 2H**, **I**, **K**, **L**).

Synchrony due to putative gap junctions or common synaptic input is rare

The presence of a minority of pairs with highly positive or negative spike count correlations suggests that at least some LC single units are correlated. Their synchronized activity could be due to common synaptic drive or electrotonic coupling (*25-27*). We assessed this possibility by measuring cross-correlograms between spike trains of single unit pairs. We observed coincident spiking on the timescale of 10's of msec as well as of less than 1 msec, which we respectively term "network interactions" (unit pairs driven presumably by common synaptic input) and putative "gap junction interactions" (unit pairs with possible electrotonic coupling). **Figure 3A** provides three examples of each type of interaction.

We found that only 13% of unit pairs had significant cross-correlations during spontaneous activity (**Figure 3B**). Of those correlated unit pairs, 60% had "network interactions" (synchrony on a timescale of 10's of milliseconds), while 13% had putative "gap junction interactions" (synchrony on a timescale of less than a millisecond), and the remaining 27% of correlated pairs had both network and gap junction interactions (**Figure 3B**). Robust reciprocal interaction between pairs of single units (e.g., unit A significantly increases its spike count after unit B spikes and unit B also significantly increases its spike count after unit A spikes) would provide a mechanism for highly uniform and synchronous firing in the LC nucleus. Out of 3,164 pairs, 254 (8.0%) had significant reciprocal interactions of either network or gap junction type. For each type of functional coupling, the proportion of reciprocal interactions was approximately 40%.

In general, a larger proportion of pairs of narrow units had significant network interactions in comparison to pairs of wide units and pairs of mixed unit types (**Figure 3B**). This finding is consistent with higher spike count correlations between narrow units (**Figure 2D**). Network interactions, just like spike count correlations, did not depend on the distance between the unit pairs and therefore occurred with similar frequency throughout the LC nucleus (**Figure 3C**). Furthermore, spike count correlations were higher between pairs with network interactions in comparison to pairs with gap junction interactions and pairs without significant cross-correlations

(**Supplementary Figure 4**). These results are consistent with network interactions reflecting common synaptic input. We next assessed the dynamics of this interaction by examining the peak times of the cross-correlograms for pairs with a significant network interaction. In the example cross-correlograms with significant network interactions (**Figure 3A**), there is a notable diversity in the timing of the interaction in different pairs. The interaction in **Figure 3A1** was centered at 0 msec, while interactions between other pairs occurred before 0 msec (**Figure 3A2**) or after 0 msec (**Figure 3A3**). Across the population of all pairs with significant network interactions, the peak timings of the interactions were spread over ±70 msec (**Figure 3D**). The peak should be centered at 0 msec if common synaptic input jointly drives the pair (*27*). Therefore, network interactions in LC do not appear to be driven exclusively by common synaptic input.

Gap junctions mediate spatially localized and exclusively pairwise sub-millisecond synchrony

In the cerebellum, retina, and cortex, either genetic or pharmacological removal of electrotonic coupling has demonstrated that sub-millisecond cross-correlogram peaks represent synchronized spiking mediated by gap junctions (*25*, *26*, *31*). Out of the 13% of cross-correlograms that were significant, 40% indicated synchrony on the timescale of gap junctions, which is 5% of 3,164 pairs assessed. Sub-millisecond interactions between LC units fell off rapidly with the distance between units (**Figure 3C**). Prominent theories of LC function have proposed a model in which gap junctions spread synchrony throughout the LC using collections of gap junction coupled neurons (*2*, *22*, *32*). We attempted to find evidence of more than two units putatively connected by gap junctions (e.g., a unit A spike is followed in the next 0.5 – 1 msec by a unit B spike, which is followed in the next 0.5 – 1 msec by a unit C spike, and so on) by searching these specific temporal sequences of unit firing (see Supplemental Methods for details). In 2 out of 12 rats, we observed triplets of units that spiked in a consistent order over 4 msec. Only 1 triplet out of 22,100 possible triplet patterns (0.005%) was found in one rat and 4 triplets out of 1,330 possible triplet patterns (0.301%) were found in the other rat. Therefore, synchrony on the timescale of gap junctions beyond two units was negligible.

Spiking of individual LC units oscillates asynchronously at low (< 2 Hz) frequency

Synchronized rhythmic spiking of LC units could emerge from entrainment to cortical oscillations. In the cortex, these oscillations are prominent during slow wave sleep and anesthesia and

include a 1 - 2 Hz "slow oscillation" regime and <1 Hz "infra-slow oscillation" regime (*33-35*). Locus coeruleus MUA has been shown to oscillate in the slow frequency band and phase lock to the down-to-up state transition (*28-30*).

We first characterized slow oscillations in the firing rate of LC single units by calculating the power spectrum of each unit's spike train converted into a continuous spike density function (SDF). We examined the mean power spectrum across the SDF's of all 235 single units (**Figure 4A**). Surprisingly, we did not observe any distinct peak at in the slow frequency band. This result is unexpected in light of previous studies, which have found that LC MUA oscillated in this range (*28-30*). In order to understand the relationship between the activity of LC single units and cortical slow oscillations, we first compared our results with prior studies of LC MUA by merging all simultaneously recorded spike trains into a single multi-unit spike train and converting that to a SDF. In line with previous studies, we observed that LC MUA did oscillate in the slow frequency band (**Figure 4B**). Out of 8 rats with spiking during cortical slow oscillations, all 8 of the multi-unit signals were significantly phase locked (Rayleigh's Z test, $p<0.05$) to the down-to-up state transition as reflected by the phase of cortical LFP slow waves (**Figure 4C**). In spite of LC single units not exhibiting spike rate fluctuations at ~ 1 – 2 Hz (**Figure 4A**), approximately 69% of single units were significantly phase locked to the cortical slow waves. Similar proportions of each unit type (70% of wide units and 66% of narrow units) were phase locked (Fisher's Exact Test, Odds Ratio=1.23, CI=[0.470 3.202], $p=0.803$). Notably, narrow units responded significantly earlier, during the down-to-up state transition, whereas wide units responded during the beginning of up state and stopped firing rapidly before the peak of the up state (Watson-Williams test for equal circular means, $F(83)=40.959$, $p<0.0001$; **Figure 4D**).

Intriguingly, we observed strong single unit spike rate oscillations in the infra-slow frequency band (**Figure 4A**), specifically at 0.09 Hz (periods of 11 sec) and 0.4 – 0.5 Hz (periods of around 2 sec). Both unit types oscillated at these frequencies and narrow units also oscillated at around 0.1 and 0.2 Hz (**Figure 4E**). The infra-slow oscillations were coherent between pairs of units (**Figure 4F**). Strong coherence between unit pairs suggests that synchronous spiking of LC unit pairs may occur at infra-slow time scales. Therefore, we next examined the phase relationship of the spike rates oscillations between LC units in the infra-slow range. The spike rate fluctuations were easily observable in spike density functions (250 msec kernel) (**Figure 4G**). The examples illustrate the spike rates of 3 pairs of units that fluctuated at 0.4 – 0.5 Hz. The

units in each pair oscillated coherently with narrow distributions of phase differences, but only the units in Pair 2 oscillated nearly synchronously (i.e., with ~ 0 degrees of phase difference). Additional examples are presented in **Supplementary Figure 5**. At the population level (all 3,164 pairs), the mean phase relation across all pairs was not distributed around 0 (**Figure 4G**). Instead, mean phase relations across pairs were distributed uniformly for spike rate oscillations at both 0.09 Hz (Rayleigh's Z=2.531, p=0.080) and 0.4 – 0.5 Hz (Rayleigh's Z=1.074, p=0.342). These data indicate a lack of pairwise oscillatory synchrony at infra-slow frequencies.

LC single units exhibit complex population patterns and form ensembles

Although we have found multiple lines of evidence that LC single units do not respond synchronously, it is in principle possible that the LC contains smaller groups of units with synchronized activity, that is, cell ensembles. For example, we observed a minority of highly-correlated unit pairs (long right tail in the spike count distributions in **Figure 2** and 13% of pairwise cross-correlograms were significant in **Figure 3**). To explore this further, we measured the coupling of single unit spiking to the spiking of the population (all remaining units) with 1 msec resolution. Population coupling measures the number of spikes that occur in the population in the same msec as a single unit spike (*36*). During spontaneous activity, population coupling varied across individual single units. For example, the spiking of example Unit A was highly synchronous with other units in the population, whereas example Unit B was uncoupled from the population (**Figure 5A**). The Z-score at time 0 for Unit A is ~13, which indicates that each time Unit A spikes, many other units in the recorded population spike in the same 1 msec bin. On the other hand, the Z-score at time 0 for Unit B is less than 2, which indicates that other units in the population do not spike in synchrony (with millisecond precision) with unit B. The distribution of Z-scores at 0 msec across all single units indicated the presence of both uncoupled single units (34% of units had Z<2) and population coupled units (**Figure 5B**). Population coupling suggests that some sub-sets of multiple units may be synchronously active as ensembles. The distribution of population coupling did not depend on ongoing cortical state (**Supplementary Figure 6**), which, importantly, suggests that ensembles may not be the product of changes in brain state, but rather emerge from the physical connectivity of LC neurons.

Sensory stimulation is thought to evoke synchronous discharge of many LC neurons (*16*) and should therefore result in strong population coupling for most single units. It is important to note

that, even if not all units respond to a foot shock stimulus, strong population coupling is expected because population coupling measures the co-occurrence of each single unit's spikes with the spikes of *any* other unit in the entire population. Astonishingly, foot shocks did not cause coupling of a large number of single units to the population (**Figure 5C, D**), suggesting a lack of synchronous population discharge to sensory stimuli at a msec time scale.

We next attempted to detect and discriminate which LC units formed correlated sub-populations spiking together as ensembles using graph theory analysis (see Supplementary Methods). We observed ensembles in each set of simultaneously recorded units (**Figure 5E**). We identified a total of 23 ensembles, ranging from 1 to 3 per rat, and consisting of 2 to 9 units per ensemble. LC unit ensembles were spatially diffuse with member units spread throughout the LC core (**Supplementary Figure 7**). Surprisingly, the units in an ensemble often consisted of the same unit type (**Figure 5F**).

A minority of correlated single units provide targeted, rather than non-specific forebrain neuromodulation

Largely non-synchronized spiking of individual LC neurons may create a region-specific concentration gradient of forebrain NE, whereas a highly synchronized minority of LC cells may be sufficient for diffuse neuromodulation, provided that their projections are broadly distributed. We assessed the projection properties of LC cells by applying direct electrical stimulation in up to 15 forebrain sites. Projection densities, projection-specific LC firing rates, and latencies of antidromic responses were consistent with prior studies (*17*, *18*, *37*) and are summarized in **Supplementary Figure 8**.

We examined the degree to which correlated units have overlapping projection targets (**Figure 6**). Targets were defined as either individual brain regions or as zones (i.e., cortical, sub-cortical, thalamic, prefrontal, primary sensory cortex, or secondary sensory cortex). Zones were examined because prior work has indicated that LC neurons may projection to multiple, functionally-related forebrain sites (*38*). In general, correlated (either positively or negatively) unit pairs did not have any greater tendency for both units to jointly project to overlapping forebrain targets (**Figure 6A, B**). Although pairwise network interactions did not relate to the degree of target overlap between units (**Figure 6C**), pairs with gap junction interactions were

more likely to project to the same target zone (two-sided Fisher's exact test, odds ratio = 3.226, CI=[0.444 2.515], p=0.009 (**Figure 6D**).

Discussion

We presented multiple lines of evidence that challenge the long-standing view about the non-specific nature of the LC NE system, which is based on the assumptions of highly synchronous discharge of LC neurons and diffuse projections (*2-6*). We demonstrated that correlated firing of LC unit pairs is surprisingly rare. We identified two types of LC units that differed in a number of physiological properties, propensity for synchronization, relation with cortical oscillations, and latency to respond to prefrontal input. A minority (13%) population of LC neurons did indeed respond synchronously forming multiple, simultaneously active ensembles. Ensembles often consisted of the same cell type. The LC cells with synchronous spiking due to putative gap junctions provided targeted neuromodulation.

Collectively, our findings suggest that the LC may integrate afferent inputs and via diverse local circuit mechanisms create multiple, distinct—yet simultaneously active—ensembles. Such finely structured activity may underlie the previously observed ability of the LC to rapidly adapt its responses to context, novelty, and learning, as well as to switch between spontaneous (tonic) and busting (phasic) modes of spiking (*1*, *2*, *39-42*). What follows discusses potential neurophysiological mechanisms that could underlie our observations. We will also discuss the functional implications of this complex network architecture.

Mechanisms that may limit synchrony in the LC nucleus

The distance-invariance of correlated activity suggests that a potentially strongly synchronizing and non-topographical input influences the entire LC nucleus, but the rarity of correlated activity suggests this influence is somehow limited. This limitation may be due to local lateral inhibition between LC units (*43*, *44*). We observed cross-correlogram peaks due to common synaptic input that were delayed up to 70 msec. This finding may indicate that the drive toward synchrony, which derives from shared excitatory inputs (*45*), is delayed by local lateral inhibition, which contributes to an overall asynchronous state in the LC. The negative spike count correlations that we observed after sensory stimuli may reflect local lateral inhibition. Such inhibition is generated by somatic release of NE from stimulus-activated neurons onto neighboring LC

neurons, which inhibits the neighbor via alpha-2 receptors (*43*, *44*, *46*). The predominance of negative correlations after sensory stimuli, relative to spontaneous spiking, may be explained by the fact that the primary mechanism for lateral inhibition in the LC (somatic NE release) requires the high frequency of spiking associated with sensory stimuli and not spontaneous activity (*47*). Surprisingly, negative correlations were more common between unit pairs with at least one wide type unit. Given that both unit types were responsive to salient stimuli, our results suggest that wide units may respond to sensory stimuli and inhibit other LC units (narrow or wide). On the other hand, while narrow units also responded to foot shocks, they may not inhibit other units. Therefore, our results are consistent with both types of units being susceptible to local inhibition, but only discharge of wide units generating sufficient somatic NE release and causing local inhibition. One consequence of this proposed LC architecture is that LC afferents that preferentially target wide units, could have a disproportionately de-synchronizing effect on the nucleus.

Mechanisms promoting sparse synchrony

As repeatedly mentioned above, synchrony was not completely absent in the LC. A small proportion of pairwise spike count correlations and cross-correlograms were significant. Some of the synchronized pairs exhibited delayed synchrony and a comparable time delay (61±21 msec) has been observed during paired intracellular slice recordings in LC (*32*). These slice recordings revealed that delayed synchrony requires both spontaneous LC activity and gap junctions, which suggests multiple mechanisms interact, locally within the LC, to produce synchrony. Indeed, recent recordings in the retina have demonstrated that gap junctions, alone, are unable to generate synchrony and, instead, do so by interacting with shared synaptic input (*25*). Prior accounts of LC synchrony have emphasized gap junctions as the primary source of LC nucleus-wide synchrony (*2*, *22*, *32*); however, we found little evidence to support this assumption. Instead, interactions between common synaptic input, lateral inhibition, and gap junctions may promote a small amount of synchrony in the nucleus.

A synchronized minority provide targeted neuromodulation

The LC has been classically viewed as a non-specific neuromodulatory system. Two findings demonstrate targeted neuromodulation. First, unit pairs with synchronous activity on the timescale of gap junctions were more likely to project to overlapping forebrain regions. Second,

we observed limited synchrony within the LC nucleus. For example, units projecting to a single forebrain region often had near-zero spike count correlations after foot shock; the lack of synchronous spiking may preclude non-specific neuromodulation because each stimulus evokes NE release from different units with different forebrain targets.

Novel implications for neuromodulation of global brain states

Given previous studies of LC MUA and the commonly accepted notion of synchronous discharge, it was expected that LC neurons would be synchronously entrained to cortical slow oscillations. However, our recordings demonstrate that LC single units responded only intermittently across slow oscillation cycles.

Different unit types responded at different times in the slow oscillation cycle, suggesting cell-type specific mechanisms could contribute to generating cortical up states. Narrow units responded during the down-to-up state transition, while wide units responded shortly after the initiation of the up state and rapidly ceased firing shortly after the up state began. Prior studies reported that LC MUA was phase locked to the down-to-up state transition (*29*, *30*). The higher firing rate of narrow units may make larger contribution to MUA, leading to this conclusion when examining MUA.

We also detected a novel oscillatory mode of LC single unit activity. Spike count oscillated at infra-slow frequencies (0.09 Hz and 0.4 - 0.5 Hz). Infra-slow oscillations have been detected in targets of LC projections, for example, in cortical neuron membrane potentials and cortical LFP, EEG, and fMRI BOLD signals (*33-35*, *48-50*). These cortical fMRI BOLD, EEG, and LFP oscillations serve to dynamically enhance communication between some networks while segregating others, thus forming the so-called resting state networks that underlie cognitive functioning (*33*, *51-53*). Researchers studying global brain activity have speculated that the LC may be responsible for cortex-wide infra-slow oscillations and the formation of resting state networks (*33*, *54-56*). Here, we demonstrate that individual LC neurons spiking oscillates at such frequencies and support prior speculation that the LC generates resting state networks (*33*, *54-56*) and modulates the engagement and disengagement of task-related networks (*2*, *57*).

The uniqueness of the LC in comparison to the dopaminergic neuromodulatory system

Our work demonstrates that LC NE neurons respond in a fundamentally different pattern in comparison to the dopamine neuromodulatory system, which is thought share functional similarity with the NE system in terms of regulating arousal, responding to salient stimuli, and influencing learning and decision-making (*5*, *58-61*). Spike count correlation coefficients between dopamine neurons are approximately 0.5, demonstrating that the dopamine system conveys a highly redundant and uniform signal to its forebrain targets (*62-65*).

Our findings provide single unit evidence demonstrating that, contrary to widely-held views (*2-6*), the LC may convey a more complex and differentiated signal to the forebrain. Nevertheless, our data also support a notion that global neuromodulation does occur. It is estimated that the unmyelinated axons of LC neurons reduce temporal fidelity of spike transmission, such that LC forebrain targets are exposed to NE release changes on a time scale of 100's of msec; furthermore, NE may not be cleared from extracellular space for a few seconds (*11*, *66*). However, asynchronous infra-slow oscillations in LC activity may produce region-specific NE gradients on much slower time scales (10's of seconds). Moreover, NE concentration gradients may be produced by finely structured activity, including gap junction synchronized neurons providing targeted neuromodulation, correlated activity within cell type-specific ensembles, and many uncorrelated pairs with non-specific projections. These results suggest that the LC NE neuromodulatory system is differentiated to a larger extent than previously thought, which may allow a more nuanced role in theories of systems and cognitive neuroscience.

Conflicts of interest

The authors declare no competing financial interests.

Author contributions

N.K.T., N.K.L., O.E. - conceived of the project; N.K.T., O.E. – experimental design; N.K.T., S.P., N.K.L., O.E. – analysis design; N.K.T., R.N. - collected data; N.K.T. - analyzed data; N.K.T., O.E. - wrote the paper; all authors - edited the paper.

Acknowledgements

We thank Axel Oeltermann and Eduard Krampe for technical assistance with stimulating electrodes, Joachim Werner for technical support, Dr. Henry Evrard for expertise in immunohistochemistry, and Marcel Hertl, Felicitas Horn, Jennifer Smuda, and Katalin Kalya for assistance with histology. We thank Dr. Susan Sara for comments on the paper. This research was supported by the European Union's Marie Curie Fellowship in the FP7 funding scheme to N.K.T. (PIIF-GA-2012-331122) and the European Union's FET Open in the FP7 funding scheme (SICODE) to S.P., O.E., and N.K.L.

References

1. S. J. Sara, S. Bouret, Orienting and reorienting: the locus coeruleus mediates cognition through arousal. *Neuron* **76**, 130–141 (2012).
2. G. Aston-Jones, J. D. Cohen, An integrative theory of locus coeruleus-norepinephrine function: adaptive gain and optimal performance. *Annu Rev Neurosci* **28**, 403–450 (2005).
3. G. Aston-Jones, M. Ennis, V. A. Pieribone, W. T. Nickell, M. T. Shipley, The brain nucleus locus coeruleus: restricted afferent control of a broad efferent network. *Science* **234**, 734–737 (1986).
4. C. W. Berridge, B. D. Waterhouse, The locus coeruleus-noradrenergic system: modulation of behavioral state and state-dependent cognitive processes. *Brain Res Brain Res Rev* **42**, 33–84 (2003).
5. K. D. Harris, A. Thiele, Cortical state and attention. *Nat Rev Neurosci* **12**, 509–523 (2011).
6. G. Aston-Jones, F. E. Bloom, Activity of norepinephrine-containing locus coeruleus neurons in behaving rats anticipates fluctuations in the sleep-waking cycle. *J Neurosci* **1**, 876–886 (1981).
7. E. Eldar, J. D. Cohen, Y. Niv, The effects of neural gain on attention and learning. *Nature Publishing Group* **16**, 1146–1153 (2013).
8. S.-H. Lee, Y. Dan, Neuromodulation of brain states. *Neuron* **76**, 209–222 (2012).
9. P. Dayan, A. J. Yu, Phasic norepinephrine: a neural interrupt signal for unexpected events. *Network* **17**, 335–350 (2006).
10. T. H. Donner, S. Nieuwenhuis, Brain-wide gain modulation: the rich get richer. *Nat Neurosci* **16**, 989–990 (2013).
11. M. L. Mundorf *et al.*, Catecholamine release and uptake in the mouse prefrontal cortex. *J Neurochem* **79**, 130–142 (2008).
12. L. A. Schwarz *et al.*, Viral-genetic tracing of the input-output organization of a central noradrenaline circuit. *Nature* (2015), doi:10.1038/nature14600.
13. K. Mitchell, A. F. Oke, R. N. Adams, In vivo dynamics of norepinephrine release-reuptake in multiple terminal field regions of rat brain. *J Neurochem* **63**, 917–926 (1994).
14. P. Room, F. Postema, J. Korf, Divergent axon collaterals of rat locus coeruleus neurons: demonstration by a fluorescent double labeling technique. *Brain Research* **221**, 219–230 (1981).
15. M. Ishimatsu, J. T. Williams, Synchronous activity in locus coeruleus results from dendritic interactions in pericoerulear regions. *J Neurosci* **16**, 5196–5204 (1996).
16. G. Aston-Jones, F. E. Bloom, Norepinephrine-containing locus coeruleus neurons in behaving rats exhibit pronounced responses to non-noxious environmental stimuli. *J Neurosci* **1**, 887–900 (1981).
17. J. M. Kebschull *et al.*, High-Throughput Mapping of Single-Neuron Projections by Sequencing of Barcoded RNA. *Neuron* **91**, 975–987 (2016).
18. D. J. Chandler, W.-J. Gao, B. D. Waterhouse, Heterogeneous organization of the locus coeruleus projections to prefrontal and motor cortices. *Proceedings of the National Academy of Sciences* **111**, 6816–6821 (2014).
19. J. N. Crawley, J. W. Maas, R. H. Roth, Biochemical evidence for simultaneous activation of multiple locus coeruleus efferents. *Life Sciences* **26**, 1373–1378 (1980).
20. J. H. Kim *et al.*, Selectivity of Neuromodulatory Projections from the Basal Forebrain and Locus Ceruleus to Primary Sensory Cortices. *Journal of Neuroscience* **36**, 5314–5327 (2016).

21. K. Watabe, *Mode of neuronal interaction in rat locus coeruleus.* (Archives italiennes de biologie, 1980).
22. M. Usher, J. D. Cohen, D. Servan-Schreiber, J. Rajkowski, G. Aston-Jones, The role of locus coeruleus in the regulation of cognitive performance. *Science* **283**, 549–554 (1999).
23. S. E. Loughlin, S. L. Foote, R. Grzanna, Efferent projections of nucleus locus coeruleus: morphologic subpopulations have different efferent targets. *Neuroscience* **18**, 307–319 (1986).
24. R. Grzanna, M. E. Molliver, The locus coeruleus in the rat: An immunohistochemical delineation. *Neuroscience* **5**, 21–40 (1980).
25. S. Trenholm *et al.*, Nonlinear dendritic integration of electrical and chemical synaptic inputs drives fine-scale correlations. *Nat Neurosci* **17**, 1759–1766 (2014).
26. I. van Welie, A. Roth, S. S. N. Ho, S. Komai, M. Häusser, Conditional Spike Transmission Mediated by Electrical Coupling Ensures Millisecond Precision-Correlated Activity among Interneurons In Vivo. *Neuron* **90**, 810–823 (2016).
27. D. H. Perkel, G. L. Gerstein, G. P. Moore, Neuronal Spike Trains and Stochastic Point Processes. II. Simultaneous spike trains. *Biophys J* **7**, 419–440 (1967).
28. R. Lestienne, A. Hervé-Minvielle, D. Robinson, L. Briois, S. J. Sara, Slow oscillations as a probe of the dynamics of the locus coeruleus-frontal cortex interaction in anesthetized rats. *J Physiol Paris* **91**, 273–284 (1997).
29. O. Eschenko, C. Magri, S. Panzeri, S. J. Sara, Noradrenergic Neurons of the Locus Coeruleus Are Phase Locked to Cortical Up-Down States during Sleep. *Cerebral Cortex* (2011), doi:10.1093/cercor/bhr121.
30. H. Safaai, R. Neves, O. Eschenko, N. K. Logothetis, S. Panzeri, Modeling the effect of locus coeruleus firing on cortical state dynamics and single-trial sensory processing. *Proceedings of the National Academy of Sciences* **112**, 12834–12839 (2015).
31. J. R. Gibson, M. Beierlein, B.W. Connors, Two networks of electrically coupled inhibitory neurons in neocortex. *Nature* **402**, 75–79 (1999).
32. V. A. Alvarez, C. C. Chow, E. J. Van Bockstaele, J. T. Williams, Frequency-dependent synchrony in locus ceruleus: role of electrotonic coupling. *Proc Natl Acad Sci USA* **99**, 4032–4036 (2002).
33. D. A. Leopold, Y. Murayama, N. K. Logothetis, Very slow activity fluctuations in monkey visual cortex: implications for functional brain imaging. *Cereb Cortex* **13**, 422–433 (2003).
34. M. Steriade, A. Nuñez, F. Amzica, A novel slow (. *J Neurosci* **13**, 3252–3265 (1993).
35. A. W. Chan, M. H. Mohajerani, J. M. LeDue, Y. T. Wang, T. H. Murphy, Mesoscale infraslow spontaneous membrane potential fluctuations recapitulate high-frequency activity cortical motifs. *Nat Commun* **6**, 7738 (2015).
36. M. Okun *et al.*, Diverse coupling of neurons to populations in sensory cortex. *Nature* **521**, 511–515 (2015).
37. J. H. Morrison, M. E. Molliver, R. Grzanna, Noradrenergic innervation of cerebral cortex: widespread effects of local cortical lesions. *Science* **205**, 313–316 (1979).
38. K. L. Simpson *et al.*, Lateralization and functional organization of the locus coeruleus projection to the trigeminal somatosensory pathway in rat. *J Comp Neurol* **385**, 135–147 (1997).
39. A. Vankov, A. Hervé-Minvielle, S. J. Sara, Response to novelty and its rapid habituation in locus coeruleus neurons of the freely exploring rat. *Eur J Neurosci* **7**, 1180–1187 (1995).

40. G. Aston-Jones, J. Rajkowski, P. Kubiak, Conditioned responses of monkey locus coeruleus neurons anticipate acquisition of discriminative behavior in a vigilance task. *Neuroscience* **80**, 697–715 (1997).
41. J. Rajkowski, H. Majczynski, E. Clayton, G. Aston-Jones, Activation of monkey locus coeruleus neurons varies with difficulty and performance in a target detection task. *Journal of Neurophysiology* **92**, 361–371 (2004).
42. S. J. Sara, M. Segal, Plasticity of sensory responses of locus coeruleus neurons in the behaving rat: implications for cognition. *Prog Brain Res* (1991).
43. M. Ennis, G. Aston-Jones, Evidence for self- and neighbor-mediated postactivation inhibition of locus coeruleus neurons. *Brain Research* **374**, 299–305 (1986).
44. G. K. Aghajanian, J. M. Cedarbaum, R. Y. Wang, Evidence for norepinephrine-mediated collateral inhibition of locus coeruleus neurons. *Brain Research* **136**, 570–577 (1977).
45. M. Ennis, G. Aston-Jones, Activation of locus coeruleus from nucleus paragigantocellularis: a new excitatory amino acid pathway in brain. *J Neurosci* **8**, 3644–3657 (1988).
46. A. Lee, D. L. Rosin, E. J. Van Bockstaele, alpha2A-adrenergic receptors in the rat nucleus locus coeruleus: subcellular localization in catecholaminergic dendrites, astrocytes, and presynaptic axon terminals. *Brain Research* **795**, 157–169 (1998).
47. H.-P. Huang *et al.*, Long latency of evoked quantal transmitter release from somata of locus coeruleus neurons in rat pontine slices. *Proceedings of the National Academy of Sciences* **104**, 1401–1406 (2007).
48. S. Vanhatalo *et al.*, Infraslow oscillations modulate excitability and interictal epileptic activity in the human cortex during sleep. *Proc Natl Acad Sci USA* **101**, 5053–5057 (2004).
49. G. Buzsáki, A. Draguhn, Neuronal oscillations in cortical networks. *Science* **304**, 1926–1929 (2004).
50. P. Lakatos, An Oscillatory Hierarchy Controlling Neuronal Excitability and Stimulus Processing in the Auditory Cortex. *Journal of Neurophysiology* **94**, 1904–1911 (2005).
51. W.-J. Pan, G. J. Thompson, M. E. Magnuson, D. Jaeger, S. Keilholz, Infraslow LFP correlates to resting-state fMRI BOLD signals. *NeuroImage* **74**, 288–297 (2013).
52. T. Hiltunen, J. Kantola, Infra-Slow EEG Fluctuations Are Correlated with Resting-State Network Dynamics in fMRI. *J Neurosci* **34**, 356–362 (2014).
53. M. D. Fox, A. Z. Snyder, J. L. Vincent, M. Corbetta, D. C. Van Essen, M. E. Raichle, The human brain is intrinsically organized into dynamic, anticorrelated functional networks. *Proc Natl Acad Sci USA* **102**, 9673–9678 (2005).
54. P. J. Drew, J. H. Duyn, E. Golanov, D. Kleinfeld, Finding coherence in spontaneous oscillations. *Nat Neurosci* **11**, 991–993 (2008).
55. J. E. Sussmann *et al.*, White matter abnormalities in bipolar disorder and schizophrenia detected using diffusion tensor magnetic resonance imaging. *Bipolar Disord* **11**, 11–18 (2009).
56. M. Mittner, G. E. Hawkins, W. Boekel, B. U. Forstmann, A Neural Model of Mind Wandering. *Trends in Cognitive Sciences* **20**, 570–578 (2016).
57. S. Bouret, S. J. Sara, Network reset: a simplified overarching theory of locus coeruleus noradrenaline function. *Trends in Neurosciences* **28**, 574–582 (2005).
58. B. Noudoost, T. Moore, The role of neuromodulators in selective attention. *Trends in Cognitive Sciences*, 1–7 (2011).
59. T. W. Robbins, Arousal systems and attentional processes. *Biological Psychology* **45**, 57–71 (1997).

60. S. J. Sara, The locus coeruleus and noradrenergic modulation of cognition. *Nat Rev Neurosci* **10**, 211–223 (2009).
61. A. Eban-Rothschild, G. Rothschild, W. J. Giardino, J. R. Jones, L. de Lecea, VTA dopaminergic neurons regulate ethologically relevant sleep–wake behaviors. *Nat Neurosci* **19**, 1356–1366 (2016).
62. Y. Kim, J. Wood, B. Moghaddam, Coordinated activity of ventral tegmental neurons adapts to appetitive and aversive learning. *PLoS ONE* **7**, e29766 (2012).
63. N. Eshel, J. Tian, M. Bukwich, N. Uchida, Dopamine neurons share common response function for reward prediction error. *Nat Neurosci* **19**, 479–486 (2016).
64. M. Joshua *et al.*, Synchronization of Midbrain Dopaminergic Neurons Is Enhanced by Rewarding Events. *Neuron* **62**, 695–704 (2009).
65. M. Watabe-Uchida, L. Zhu, S. K. Ogawa, A. Vamanrao, N. Uchida, Whole-Brain Mapping of Direct Inputs to Midbrain Dopamine Neurons. *Neuron* **74**, 858–873 (2012).
66. G. Aston-Jones, M. Segal, F. E. Bloom, Brain aminergic axons exhibit marked variability in conduction velocity. *Brain Research* **195**, 215–222 (1980).

Figures

Rat Identification	Number of single units	Number (%) of narrow type	Number (%) of wide type	Spontaneous activity	Tested PFC stimulation-evoked orthrodromic spikes	Tested multi-site forebrain stimulation-evoked antidromic spikes
959.1	7	5 (71)	2 (29)	Y	Y	N
980.4	9	9 (100)	0 (0)	Y	Y	N
105.1	5	0 (0)	5 (100)	Y	Y	N
105.2	52	10 (19)	42 (81)	Y	Y	N
109.1	21	0 (0)	21 (100)	Y	Y	N
134.2	15	0 (0)	15 (100)	Y	Y	Y
259.1	19	0 (0)	18 (100	Y	Y	Y
259.2	27	4 (15)	23 (85)	Y	Y	Y
263.2	36	2 (6)	34 (94)	Y	Y	Y
286.3	8	3 (38)	5 (62)	Y	Y	Y
288.1	6	0 (0)	6 (100)	Y	Y	Y
288.2	30	1 (3.3)	29 (96.7)	Y	Y	Y
	Total					
	235					

Table 1. The number of LC single units recorded and experimental conditions tested in each rat.

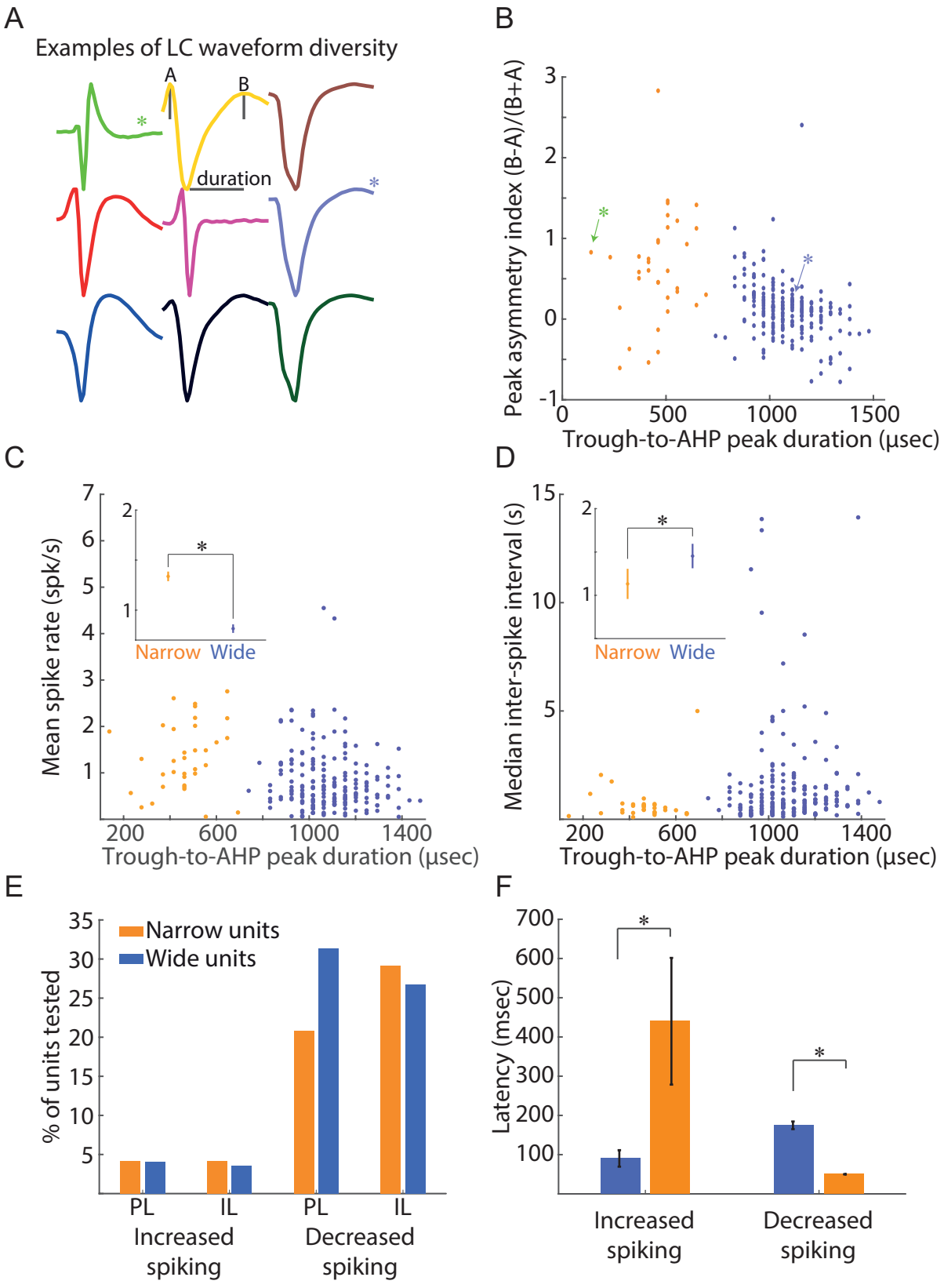

Figure 1. Distinct populations of LC single units were separable by waveform shape, spike rate, and responsiveness to prefrontal cortex stimulation. **(A)** The average waveforms of 9 example units illustrate the diversity of waveform shapes in the LC. **(B)** Units were separable based on the waveform duration and the amplitude of the after-hyperpolarization in relation to the first peak. The green and blue asterisks refer to the example waveforms in panel A with the same markings. **(C, D)** Scatter plots with the mean spontaneous spike rate (C) and inter-spike interval (D) for each isolated LC unit. The insets on C and D show the mean and standard error for each unit type. For narrow type units, spike rate was significantly higher (Mann-Whitney U test, U=4912, p=2.57e-5) and inter-spike interval was significantly shorter (Mann-Whitney U test, U=-2260, p=0.002). **(E)** A decrease in spiking was the predominant response of LC units to PFC stimulation (PL – prelimbic division, IL – infralimbic division). A similar proportion of each unit type was responsive to PFC stimulation. **(F)** The latency to increase spiking to PFC stimulation was shorter for wide units (two-way t-test, T(60)=-4.16, p=0.0001), whereas the latency to decrease spiking was longer for wide units (T(187)=3.15, p=0.002).

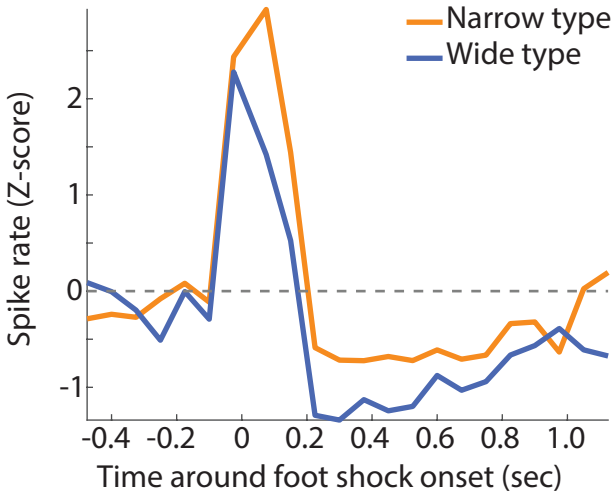

Supplementary Figure 1

Supplementary Figure 1. The bi-phasic response to foot shock stimuli did not differ between unit types. The normalized mean response profile for narrow and wide units is plotted around foot shock onset at time 0. Foot shocks were 5mA pulses delivered at 30 Hz.

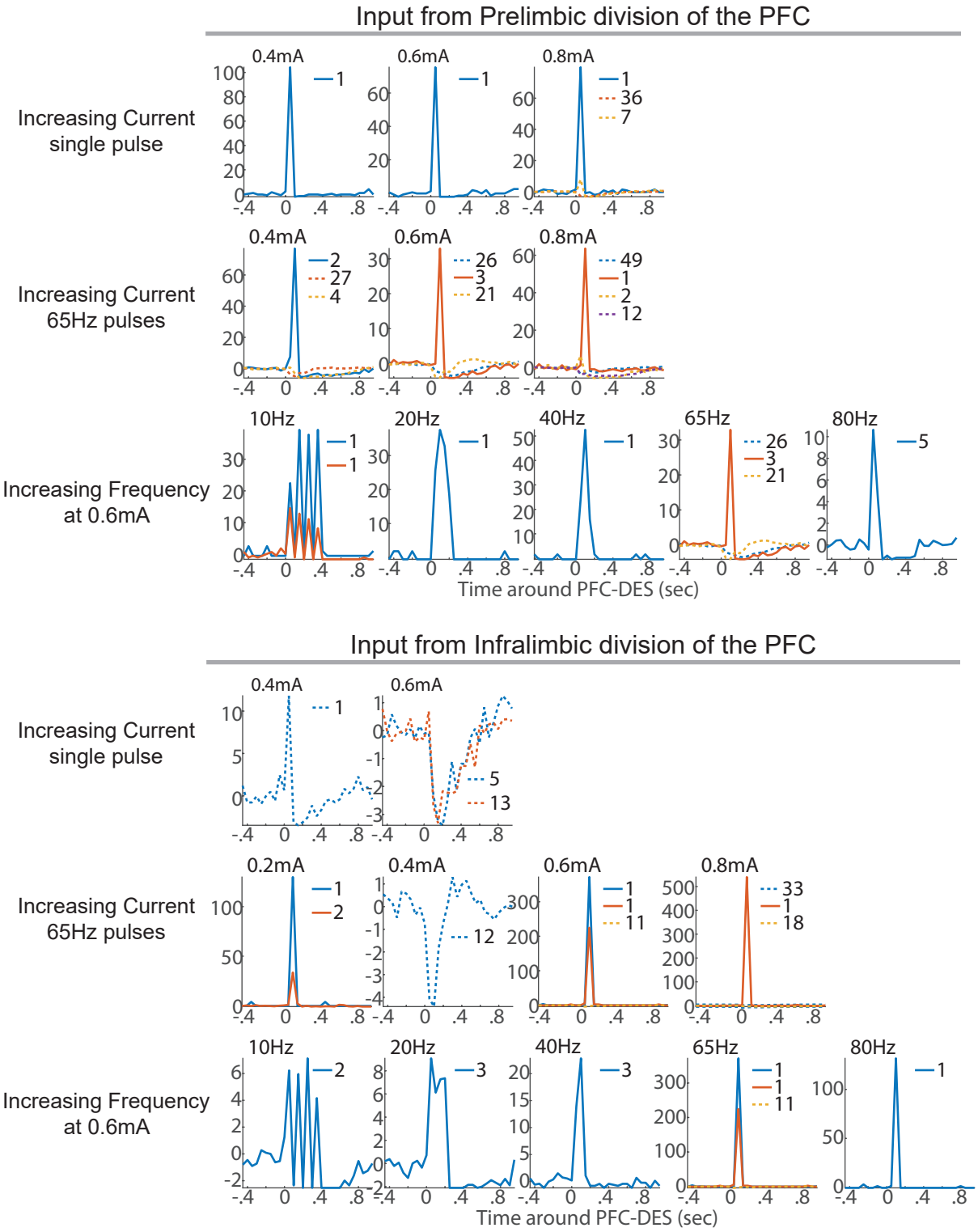

Supplementary Figure 2

Supplementary Figure 2. The PFC was stimulated at a variety of currents and frequencies (see Supplementary Materials, Methods). For each stimulation parameter, the peri-stimulus time histograms for units were grouped by k-means clustering. The units in a group were considered to be responsive if their group mean crossed a Z-score of ±2. The plots illustrate the group means for all responsive groups. Increases in spiking are plotted with solid lines and decreases in spiking are plotted with dotted lines. Each group is a different line color. The number in each legend specifies the number of units in the group. The time of stimulation onset is at time 0.

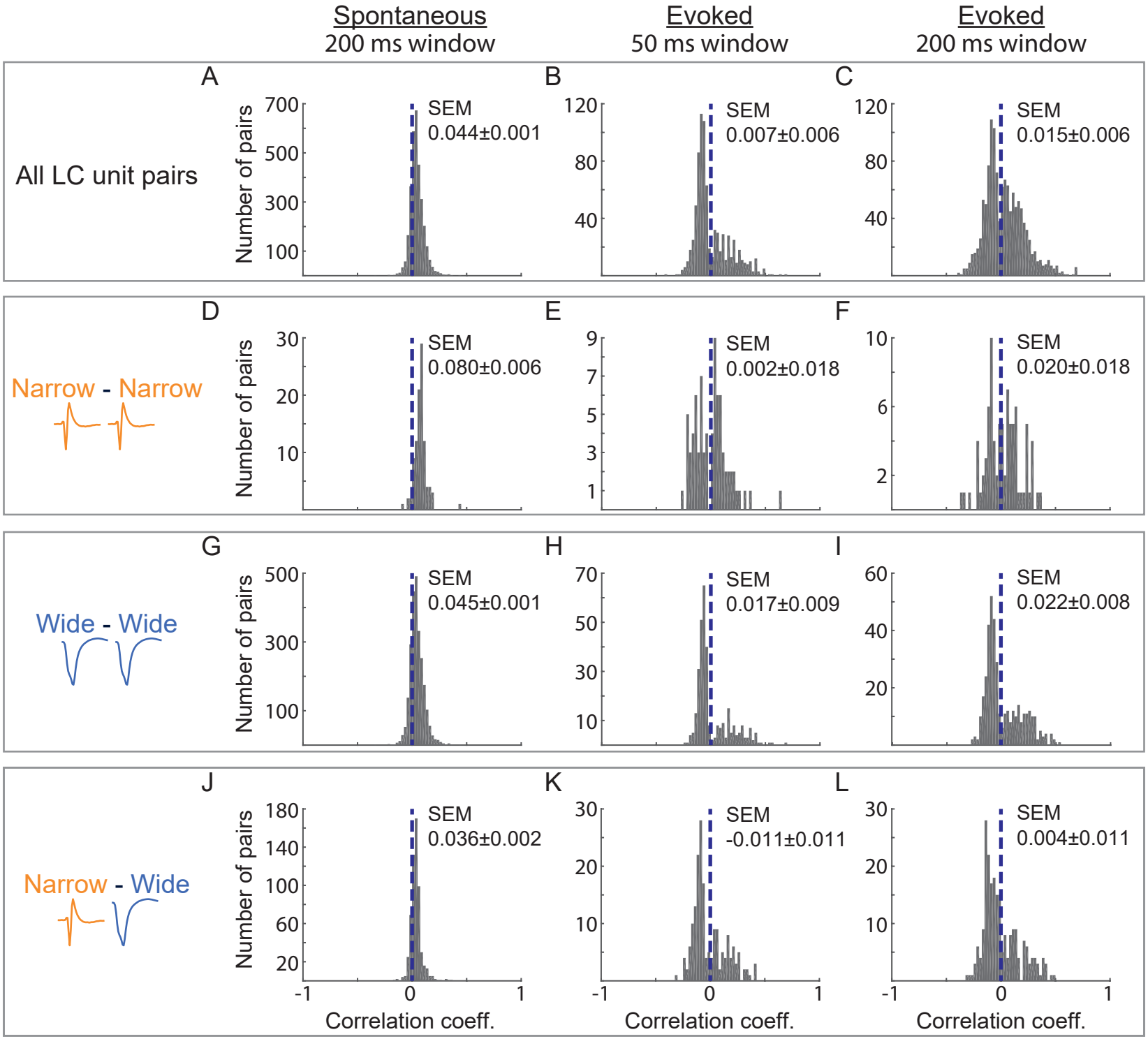
Spontaneous
200 ms window
Evoked
50 ms window
Evoked
200 ms window
A
B
C
All LC unit pairs
Number of pairs
SEM
0.044±0.001
SEM
0.007±0.006
SEM
0.015±0.006
D
E
F
Narrow - Narrow
SEM
0.080±0.006
SEM
0.002±0.018
SEM
0.020±0.018
G
H
I
Wide - Wide
SEM
0.045±0.001
SEM
0.017±0.009
SEM
0.022±0.008
J
K
L
Narrow - Wide
SEM
0.036±0.002
SEM
-0.011±0.011
SEM
0.004±0.011
Correlation coeff.
Correlation coeff.
Correlation coeff.

Figure 2

Figure 2. Pairwise spike count correlations are near zero and are anti-correlations are cell-type specific. (**A**-**C**) The distribution of spike count correlation coefficients is around zero (red line) during spontaneous spiking (**A**) or following foot shock stimulation (**B**, **C**) The spike counts were binned in 50 msec or 200 msec epochs as labeled in the figures Spike count correlations are plotted separately for pairs of narrow units (**D**-**F**), pairs of wide units (**G**-**I**), and pairs of mixed unit type (**J**-**L**). Spontaneous activity of pairs of narrow units was more correlated than other unit types (**D** versus **G** and **J**). Prominent negative correlations are apparent after evoked foot shocks in B and C. These negative correlations only occur in pairs containing a wide unit (**H**, **I**, **K**, **L**).

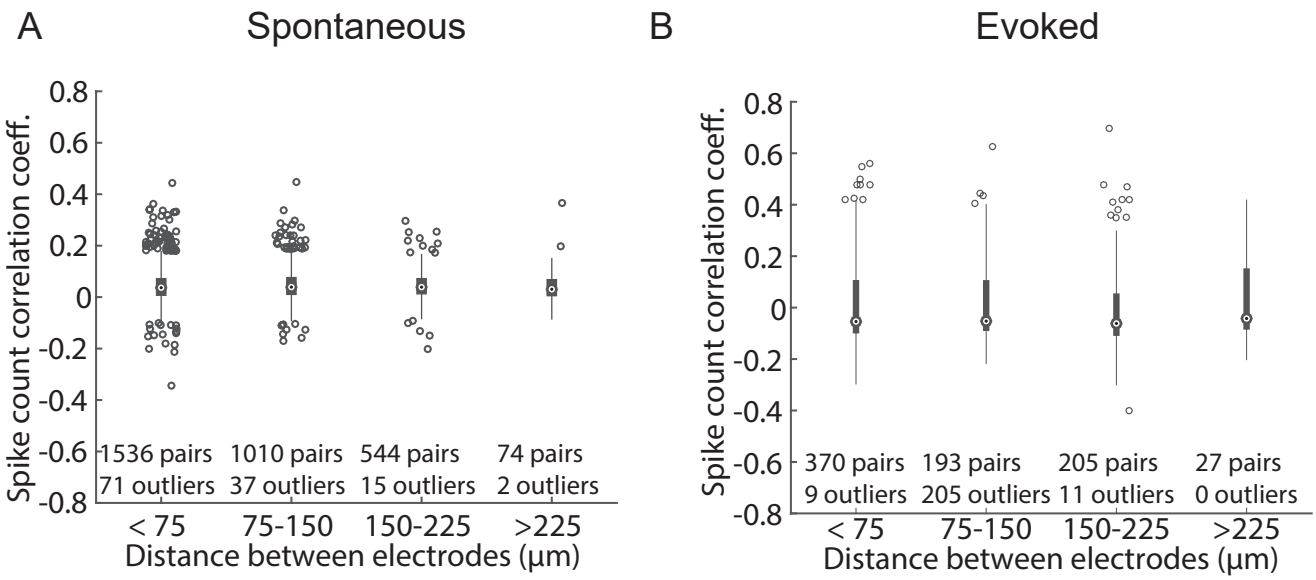

Supplementary Figure 3

Supplementary Figure 3. Spike count correlation coefficients did not depend on distance between unit pairs. The distance between units was estimated as the distance between the electrode contacts that recorded the maximal amplitude of each unit. Data are plotted as box plots.

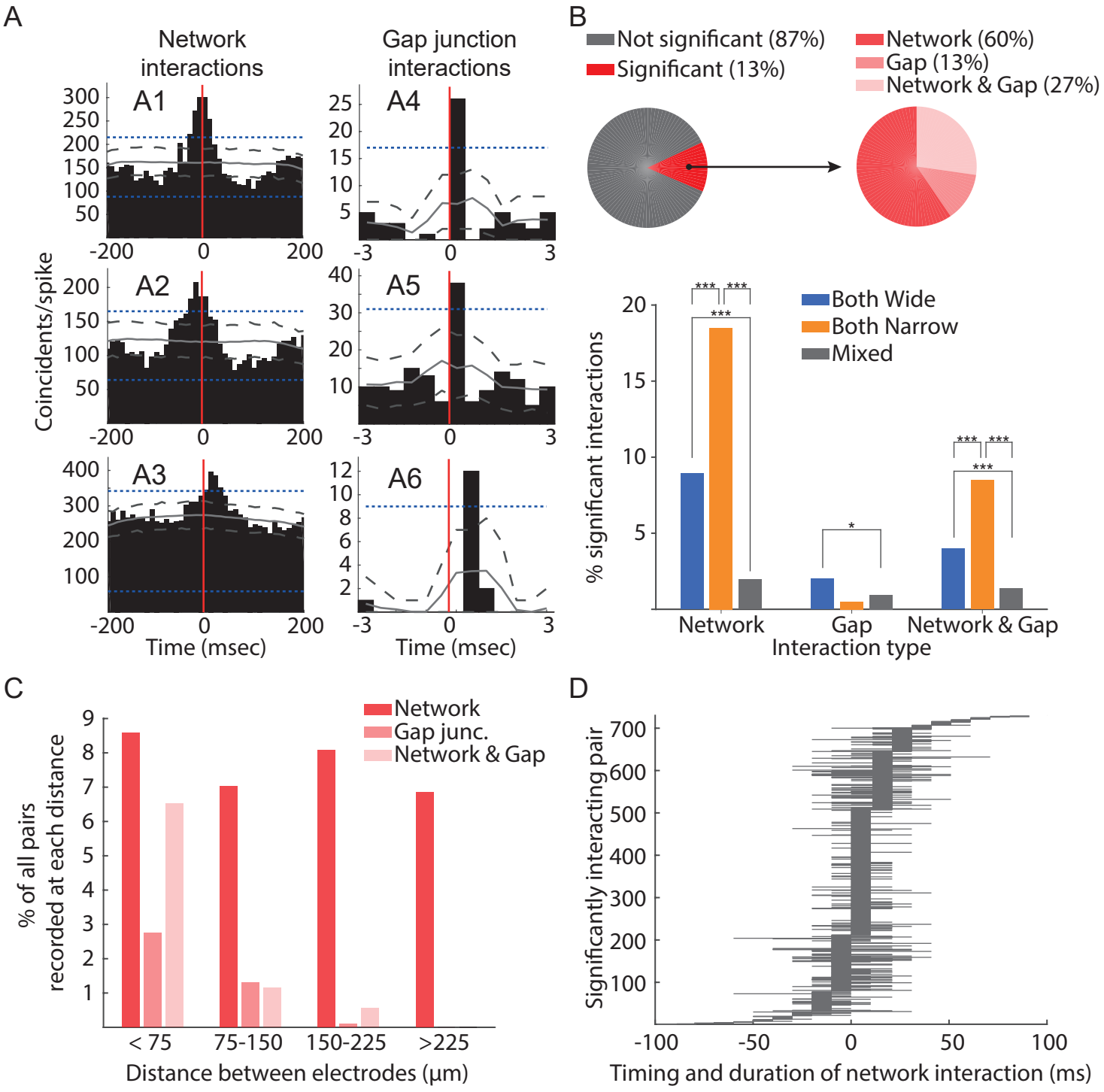

Figure 3

Figure 3. Spike train cross-correlograms indicated that interactions were rare with a synchronized minority of pairs throughout LC interacting on the timescale of network interactions and spatially-confined pairs interacting on the timescale of gap junctions. **(A)** Three example cross-correlograms with significant coincidental spiking on the timescale of network interactions (A1-A3) and gap junction interactions (A4-A6). A significant number of coincidental spikes crossed both a pairwise 1% threshold (dotted grey lines) and a 1% global threshold (dotted blue lines) obtained from a surrogate data set of 1000 cross-correlograms computed from jittered spike times (see Supplemental Materials, Methods). The mean of the 1000 surrogate cross-correlograms is a solid grey line. **(B)** A minority of cross-correlograms (13%) had a significant number of coincidental spikes in at least one bin. Out of those 13%, network interactions occurred in 60%, gap junction interactions occurred in 13%, and both types of interaction occurred in 27%. A larger percent of the pairs of narrow units had significant network interactions in comparison to pairs of wide units or pairs of both unit types. **(C)** The percent of pairs with network interactions was similar regardless of the distance between the units in the pair. On the other hand, gap junction interactions occurred only between spatially confined units. **(D)** Out of the pairs with significant network interactions, the timing of the interaction peak and the duration (continuous bins above the significance threshold) is plotted for each pair. Network interactions occurred over a broad time range. Peaks were not exclusively centered at time 0 with a symmetrically spread around time 0 (as in panel A1).

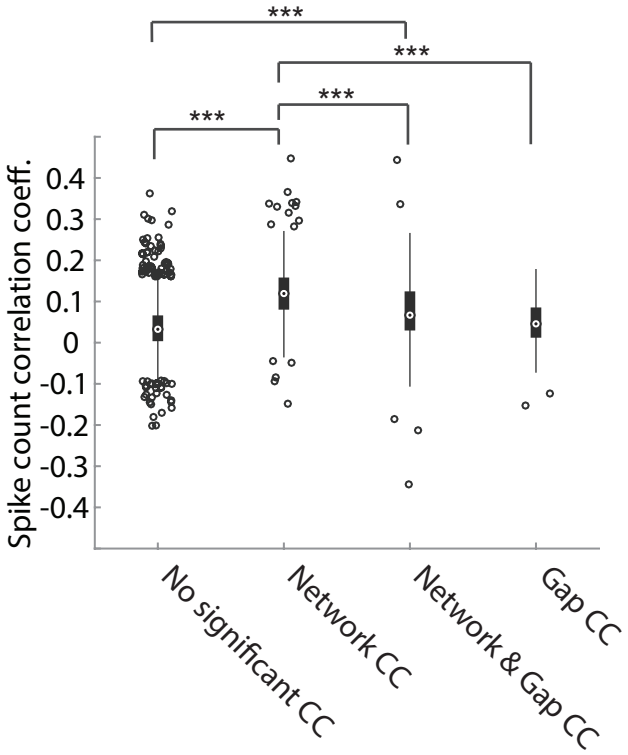

Supplementary Figure 4

Supplementary Figure 4. Pairs with network interactions have higher spike count correlations.

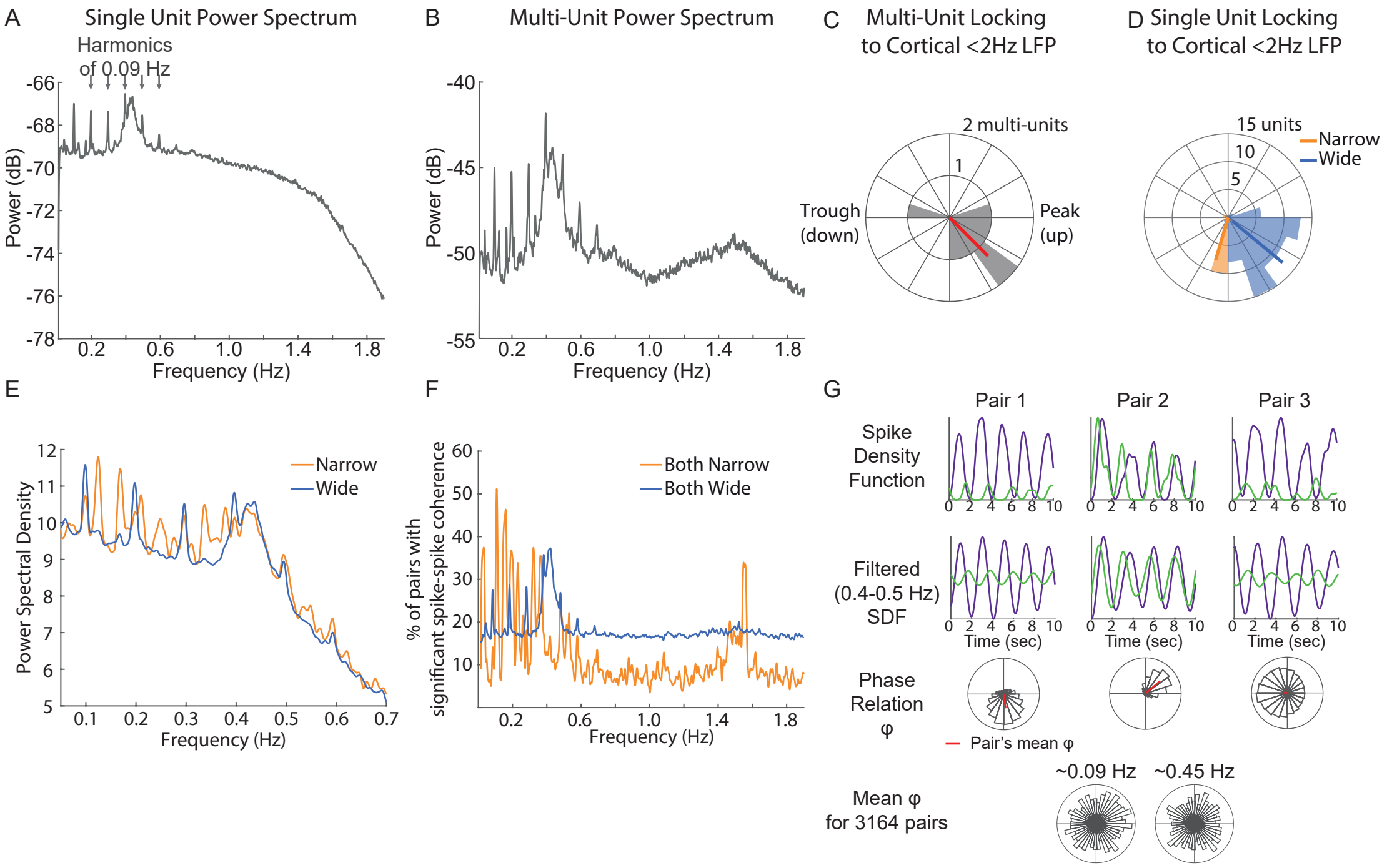
A
Single Unit Power Spectrum
Harmonics
of 0.09 Hz
Power (dB)
Frequency (Hz)
B
Multi-Unit Power Spectrum
Power (dB)
Frequency (Hz)
C
Multi-Unit Locking
to Cortical <2Hz LFP
2 multi-units
Trough
(down)
Peak
(up)
D
Single Unit Locking
to Cortical <2Hz LFP
15 units
Narrow
Wide
E
Power Spectral Density
Narrow
Wide
Frequency (Hz)
F
% of pairs with
significant spike-spike coherence
Both Narrow
Both Wide
Frequency (Hz)
G
Pair 1
Pair 2
Pair 3
Spike
Density
Function
Filtered
(0.4-0.5 Hz)
SDF
Time (sec)
Phase
Relation
φ
Pair's mean φ
Mean φ
for 3164 pairs
~0.09 Hz
~0.45 Hz

Figure 4

Figure 4. Spike rates oscillated asynchronously across individual LC units. **(A)** Single unit spike trains were converted to spike density functions and their power spectrum was calculated. The plot shows the mean power spectrum across all single units. Two oscillatory regimes at 0.09 Hz and between 0.4 and 0.5 Hz were observed in single unit spike trains. **(B)** Merging simultaneously recorded single unit spike trains into one multi-unit spike train before constructing a spike density function revealed spectral power at the infra-slow frequencies (0.09 Hz and 0.4-0.5 Hz), as well as at around1 – 2 Hz. **(C)** Multi-unit spiking was phase locked to the down-to-up state transition reflected by the phase of cortical slow waves. The polar plot is a histogram of the number of multi-units at each bin of cortical LFP phase. The red line is the mean across multi-units. **(D)** Single units were also phase locked to the cortical down-to-up state transition, in spite of not rhythmically spiking at that frequency (panel A). Narrow units responded significantly earlier than wide units during the cortical slow wave. The wide units preferentially fired at 320 degrees, whereas the mean angle for narrow units was 254 degrees (the trough, or down state, was 180 degrees and the zero-crossing between the trough and the peak was at 270 deg). **(E)** Wide and narrow units both oscillated at infra-slow frequencies (0.09 Hz and 0.4-0.5 Hz), but narrow unit spike trains had additional peak of spectral power between 0.1 and 0.2 Hz. **(F)** The spike counts of narrow and wide units fluctuated coherently at a range of infra-slow and slow frequencies. The percent of pairs with significant spike-spike coherence is plotted for pairs of narrow units and pairs of wide units. Pairs of wide units oscillated together at 0.09 Hz and 0.4-0.5 Hz. Pairs of narrow units oscillated together at different infra-slow frequencies and at approximately 1.5 Hz. **(G)** The spike rates of 3 example pairs over a 10 sec period are plotted as spike density functions (top panel) and filtered for 0.4-0.5 Hz (middle panel). The bottom panel is a histogram of the phase differences (φ) between the units' oscillations over the entire recording session. The mean φ for each example pair is marked by the red line on the polar plot. At the population level of all 3164 pairs, the mean φ across pairs are distributed across all phases. A pair was included in the population histogram is its distribution of phase relations were significantly non-uniform (Rayleigh's Test for Circular Uniformity, $p<0.05$), as in the 3 example pairs.

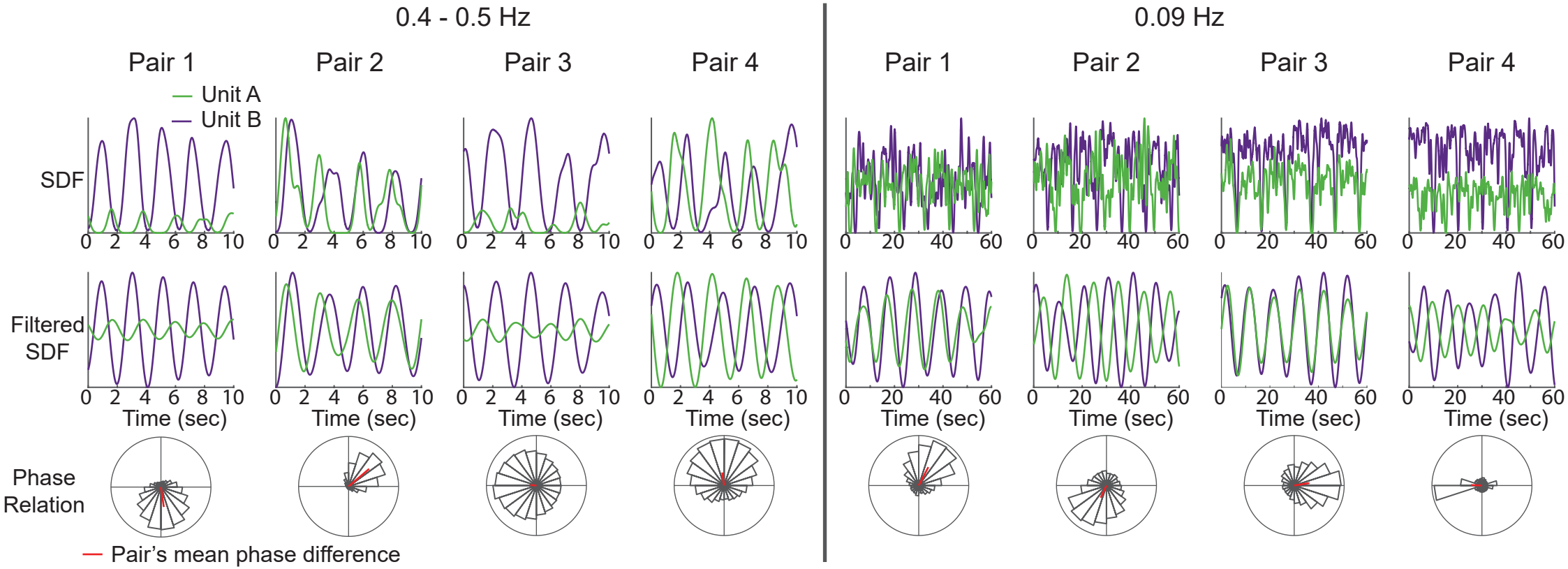

Supplementary Figure 5

Supplementary Figure 5. Examples of pairwise spike rate oscillations at 0.09 Hz and 0.4-0.5 Hz. The top and middle panels shows spike density functions over a small recording segment; the bottom panels show the phase relation between the units in the pair over the entire session. The mean phase relation for each pair is marked by the red line. All example pairs had a significantly non-uniform (Rayleigh's Test for Circular Uniformity, $p<0.05$).

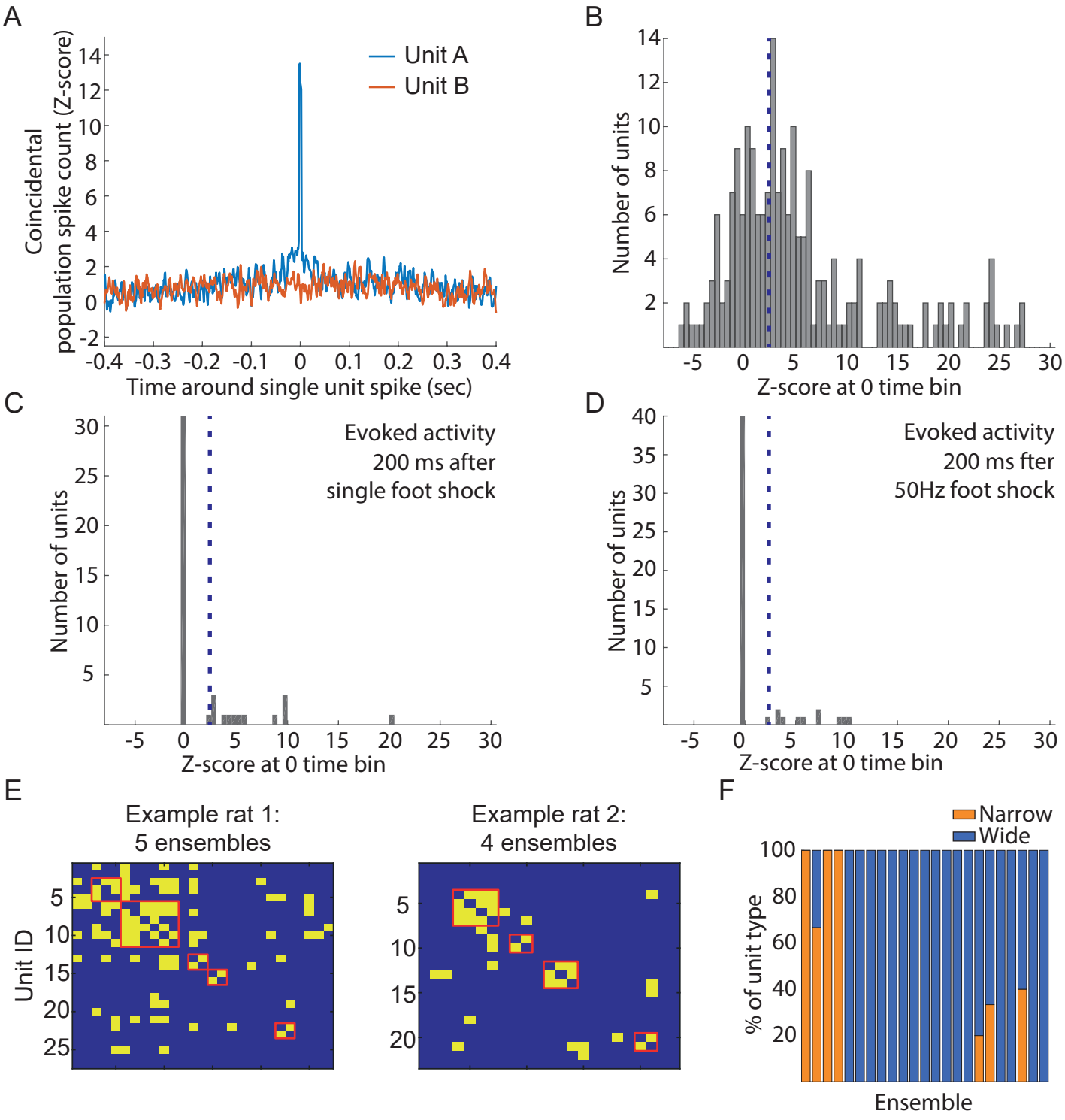

Figure 5

Figure 5. LC single units have diverse coupling to the population and organize into ensembles of homogenous unit type. **(A)** Population coupling was calculated as the cross-correlogram between each single unit and the merged spike train of all remaining single units that were simultaneously recorded. The cross-correlogram was calculated with 1 msec bins over a period of ±400 msec and Z-score normalized to the period between 300 and 400 msec (edges of the cross- correlogram). Example unit A illustrates a case of strong population coupling. Spikes of unit A coincided with spikes of many other units recorded simultaneously. Example unit B illustrates a lack of population coupling. **(B)** A histogram of the population coupling strength (Z-score at time 0) illustrates the broad range of population coupling strength across LC single units. **(C, D)** Population coupling using spikes during the 200 msec after a single foot shock (C) or after a brief train of foot shocks (5 mA pulses at 30 Hz) (D). As with spontaneous activity, many single units are not coupled to the population, with the exception of those units on the right tail of the distribution. **(E)** Two examples of ensembles detected in 2 rats. Yellow dots indicate correlated units. Red lines outline ensembles. Ensembles are defined as correlated activity between two or more single units. All simultaneously recorded single units were treated as a network with links between correlated pairs and ensembles were detected using community detection algorithms on the network (see Supplemental Materials, Methods). **(F)** The percent of each unit type making up each ensemble. Each bar is one of 23 ensembles. The majority of units in each ensemble were the same type.

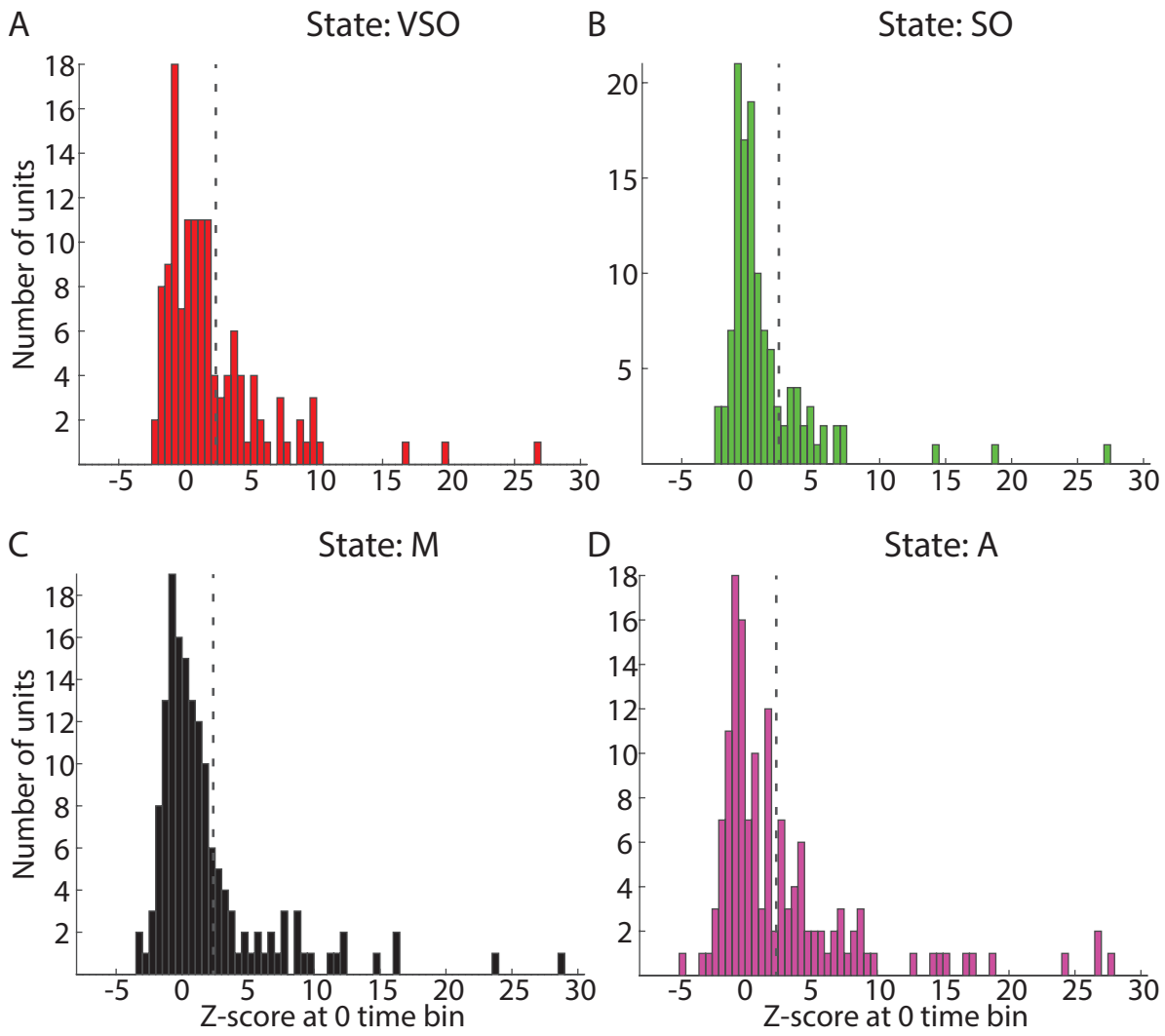

Supplementary Figure 6

Supplementary Figure 6. Population coupling did not depend on arousal state. A histogram of the population coupling strength (Z-score at time 0) is plotted for each cortical state. **(A)** The very slow oscillation state. **(B)** The slow oscillation state. **(C)** A mixture of slow oscillations and activated states. **(D)** The activated state.

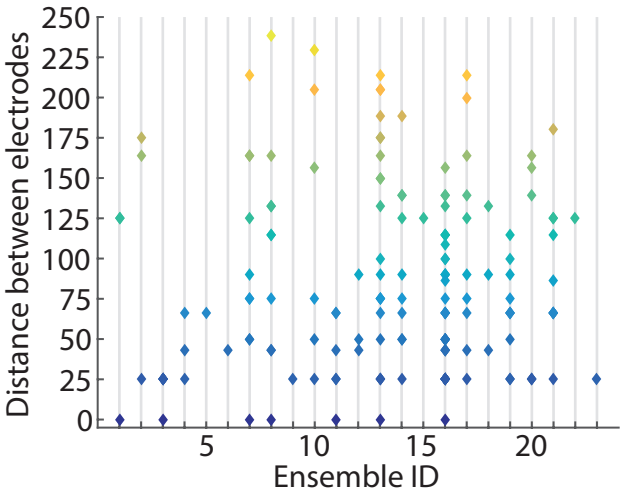

Supplementary Figure 7

Supplementary Figure 7. Ensembles are spatially diffuse. The pairwise distance between all pairs within an ensemble are plotted for all 23 ensembles. The color indicates the distance between a pair.

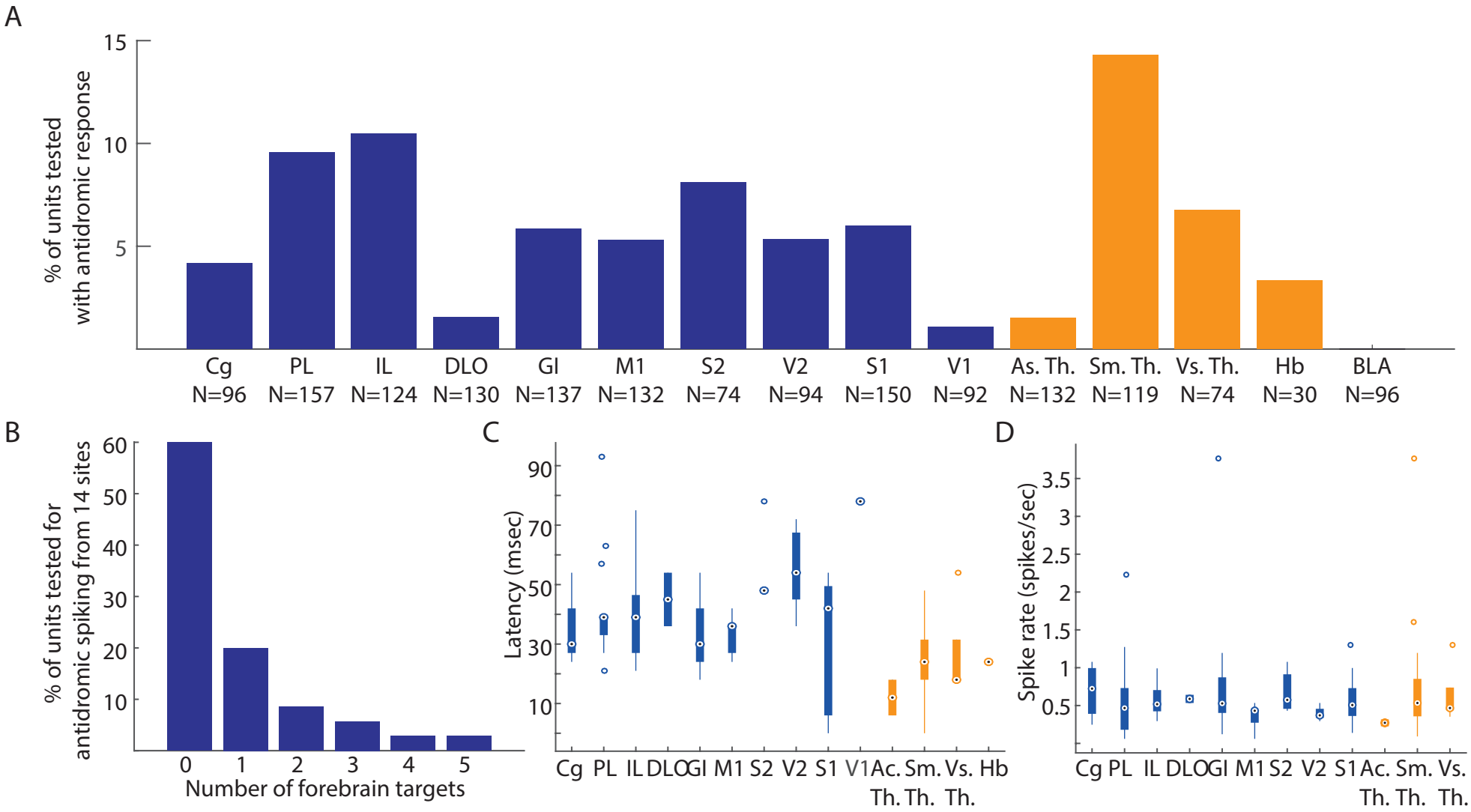

Supplementary Figure 8

Supplementary Figure 8. A summary of forebrain projection patterns and latencies. **(A)** Single units projected to a variety of forebrain sites. The y-axis shows the percent of units projecting to each site. The total number of units tested for projections to each site is written on the x-axis. Cortical regions are in blue and sub-cortical regions are in orange. **(B)** A mixture of broad (multiple targets) and selective (single target out of 15 regions tested) projection patterns were observed. Antidromic activation of units after stimulation ranged from 1 to 5 forebrain sites. Selective projections are in agreement with prior anatomical studies that traced projections of single LC neurons (*17*). The average number of projections per single unit with antidromic spiking was 2.0±0.3, which is similar to the 1.6±0.8 projection targets reported using barcoded RNA (*17*). **(C)** A box plot shows the latency antidromic spikes elicited by stimulation of different forebrain sites. The latency of antidromic responses was shorter for sub-cortical stimulation sites compared to the cortical sites and latencies for more posterior cortices were longer in comparison to more anterior cortices. This is consistent with the LC projections, which pass through thalamus before entering anterior cortex and then traveling to the posterior cortex (*37*). **(D)** The mean spike rate of LC single units did not depend on their projection target, although there was a tendency for PFC-projecting units to spike at a higher rate than M1-projecting units (M1 v.s. ACC: $T(9)=-2.18$, $p=0.063$; M1 v.s. PL: $T(20)=-1.07$, $p=0.296$; M1 v.s. IL: $T(18)=-2.282$, $p=0.035$; M1 v.s. OFC: $T(7)=-1.90$, $p=0.098$). This result is in agreement with recent study using LC slice recordings from neurons labeled with retrograde tracers injected in the OFC, PL, ACC, and M1 (*18*).

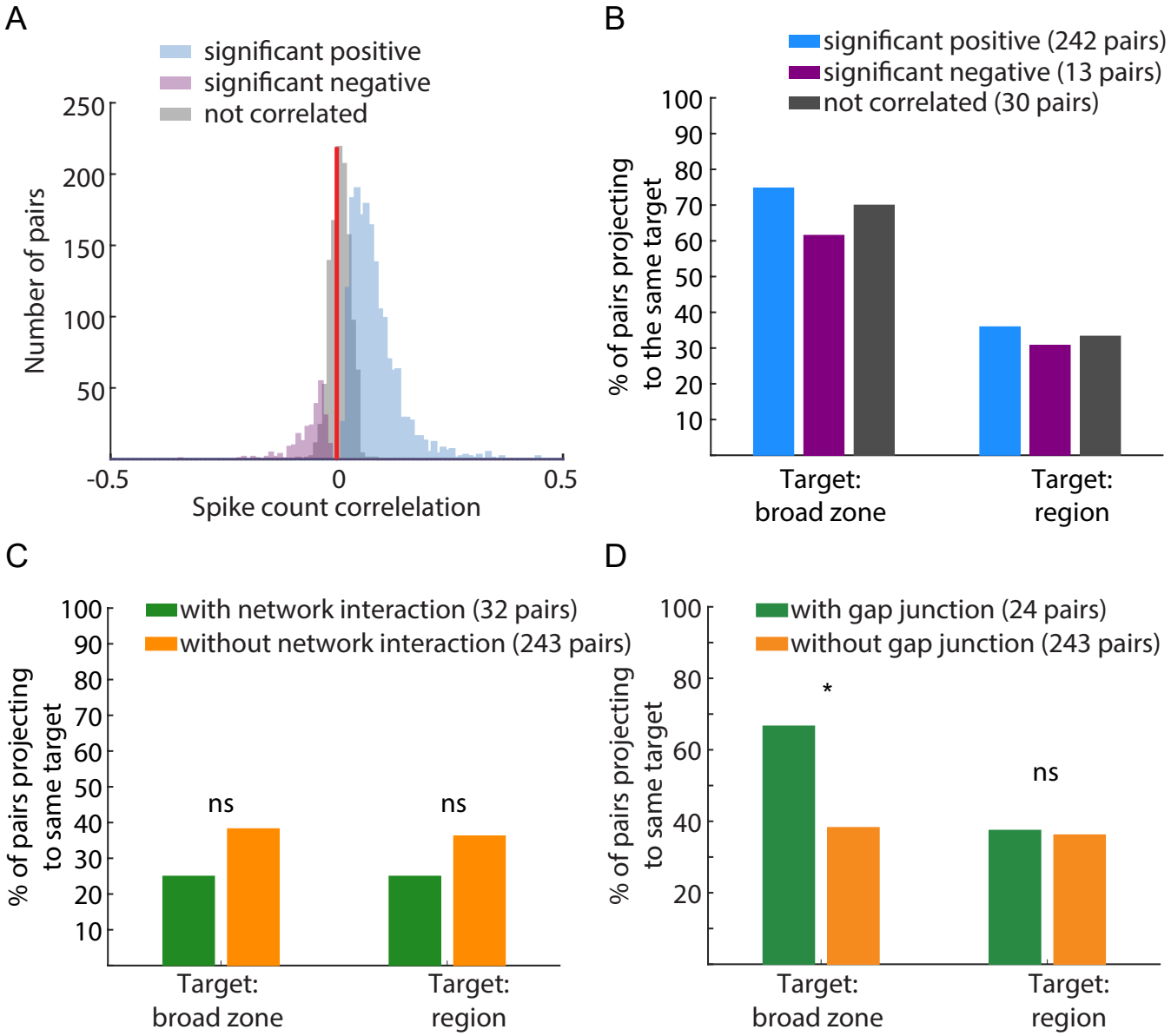
A
significant positive
significant negative
not correlated
Number of pairs
250
200
150
100
50
-0.5
0
0.5
Spike count correlelation
B
significant positive (242 pairs)
significant negative (13 pairs)
not correlated (30 pairs)
% of pairs projecting to the same target
100
90
80
70
60
50
40
30
20
10
Target: broad zone
Target: region
C
with network interaction (32 pairs)
without network interaction (243 pairs)
% of pairs projecting to same target
ns
ns
Target: broad zone
Target: region
D
with gap junction (24 pairs)
without gap junction (243 pairs)
% of pairs projecting to same target
*
ns
Target: broad zone
Target: region

Figure 6

Figure 6. The minority of unit pairs with synchrony on the timescale of gap junctions provided targeted forebrain neuromodulation. **(A)** Spike count correlations coefficients were divided into highly correlated pairs (Pearson's correlation coefficient, $p<0.001$) with positive (blue) or negative (purple)correlations. **(B)** The percent of pairs with both units jointly projecting to the same forebrain target did not differ between pairs with correlated activity (blue), anti-correlated activity (purple), and non-correlated units (grey). The percent is out of the total number of units indicated in the figure legend. **(C)** The percent of pairs with overlapping projection targets did not depend on the pair having a network interaction. **(D)** Pairs with gap junction interactions had a significantly greater likelihood of projecting to the same forebrain target zone.

Supplementary materials

1 Materials and Methods: Animal and Electrophysiology

1.1 Animals

Twelve male Sprague-Dawley rats (350 - 450 g) were used. Rats were housed in darkness from 07:00 to 19:00 hours and recordings were carried out between 13:00 and 02:00. Rats received food and water ad libitum. All experimental procedures were carried out with approval from the local authorities and in compliance with the German Law for the Protection of Animals in experimental research (Tierschutzversuchstierverordnung) and the European Community Guidelines for the Care and Use of Laboratory Animals (EU Directive 2010/63/EU).

1.2 Materials and Methods: Anesthesia and Surgical Procedures

Rats were anesthetized using an intra-peritoneal (i.p.) injection of urethane (Sigma-Aldrich, U2500). Urethane was administered at a dose of 1.5 g/kg body weight. Supplemental oxygen was administered via nose cone. The animal was placed on a heating pad and a rectal probe was used to adjust body temperature to 37C. The heart rate and blood oxygenation was measured using a pulse oximeter (Nonin Medical, Model: 8600V). The eyes were covered in ointment. The cranium was fixed in a stereotaxic apparatus. After removal of the skin, the skull was cleaned such that bregma and lambda could be visualized. The skull was leveled to 0 degrees, such that the difference between lambda and bregma was less than 0.2 mm. Craniotomies were made to access various brain regions for recording and or stimulation.

1.3 Materials and Methods: Electrophysiology

1.3.1 Stereotaxic coordinates and electrode placement

Craniotomies were made at the locations listed in the following table. Accurate electrode placement was confirmed by examining the firing properties of neurons in each brain region. In the LC, these criteria included a slow spontaneous firing rate, biphasic response to noxious sensory stimuli (foot shock), audible presence of jaw movement-responsive cells in the MeV (Mesencephalic Nucleus of Cranial Nerve V) with undetectable single units (<0.2 mV). Sensory cortical and thalamic regions were confirmed by detecting evoked multi-unit spiking after delivery of modality specific stimuli (contralateral eye illumination and whisker brushing). Electrode placements were later verified using histological examination of brain tissue sections (see section 1.5, Materials and Methods: Histology).

Region	Ref.	Anterior/Posterior (mm)	Lateral (mm)	Ventral from dura (mm)	Angle (deg)
LC	Lambda	-4.0 to -4.2	1.1 to 1.2	5.5 to 6.2	15 posterior
PL	Bregma	+3.0	0.6	3.0	none
IL	Bregma	+3.0	0.6	4.4	none
ACC	Bregma	+1.0	1.2	2.2	4 lateral
DLO	Bregma	+4.0	3.0	2.4	none
M1	Bregma	+3.0	3.0	1.6	none
GI	Bregma	+1.0	5.0	4.0	none
S1	Bregma	-1.0	5.0	1.8	none
S2	Bregma	-2.0	4.5	4.15	15 lateral
BLA	Bregma	-1.88 to -2.12	4.6 to 4.9	6.8	none
MDTh	Bregma	-3.0	1.0	5.0	2 lateral
Hb	Bregma	-3.0	1.0	4.5	2 lateral
VPMTh	Bregma	-3.0	3.0	5.6	none
DLGN	Bregma	-4.0	3.5	4.0	none
V2	Bregma	-5.0	4.8	1.2	none
V1	Bregma	-7.0	3.0	1.4	none

1.3.2 Electrodes

Stimulation of cortical and sub-cortical brain regions was conducted via tungsten electrodes with low impedance (10 - 50 kOhm) to prevent heating at the electrode tip. Tungsten electrodes with a diameter of 200 μm (FHC, Model: UEWMFGSMCNNG) were ground at the tip to lower impedance to this range. Stimulation of the PL and IL was performed using two tungsten electrodes glued side-by-side with 200 μm tip separation in the anterior-posterior axis of the brain and the IL electrode tip 1400 μm longer (ventral in the brain).

Recording from the LC used a 15 μm thick silicone probe with 32 channels (NeuroNexus, Model: A1x32-Poly3-10mm-25s-177-A32). The channels were implanted toward the anterior aspect of the brain. Each channel was separated from the neighboring channels by 25 μm. Channels were divided into 10 tetrodes with one channel overlapping per tetrode (**Supplementary Materials Figure 1A**).

1.3.3 Recording and signal acquisition

A silver wire inserted into the neck muscle was used as a reference for the electrodes. Electrodes were connected to a pre-amplifier (in-house constructed) via low noise cables. Signals were amplified (by 2000 for LC and 500 for cortical LFP) using an Alpha Omeda multi-channel processor (Alpha Omega, Model: MPC Plus). All signals were filtered with an 8KHz lowpass and a DC highpass. Signals were digitized at 24 kHz (CED, Model: Power1401mkII), and inspected and stored using Spike2 software (CED). In addition to being recorded, signals were monitored on an oscilloscope.

1.3.4 Spike detection and single unit isolation

1.3.4.1 Spike detection

The recorded signal for each channel was filtered offline with a four pole butterworth bandpass (300 - 8000 Hz). Spikes were then detected as crossings of a negative threshold that was four times the standard deviation of the channel noise. Noise was defined as the median of the rectified signal divided by 0.6745 (1). Detected spike waveforms were stored from 0.6 msec to 1.0 msec around the threshold crossing. This duration was chosen based on the known action potential duration of rat LC neurons (2,3). A 0.6 msec refractory period was used to not detect a subsequent spike during this window.

1.3.4.2 Spike clustering

Spike waveforms were clustered using an automatic clustering algorithm and then manually refined. Automated clustering was performed using Wave_Clus (1) in MATLAB (default parameters for clustering. This method uses wavelets to decompose the waveform into a simpler approximation of its shape at different frequencies (wavelet scales) and times in the waveform. Using this method, small amplitude bumps or deflections at different time points in the waveform can be used to cluster waveforms together, if they are a highly informative waveform characteristic. The benefit of this method is that these characteristic and informative waveform features may be ignored by principle components analysis (PCA) because they do not contribute much variance. After the automated sorting, manual refinement of clustering using a 3-dimensional plot of principle components or the amplitude at particular waveform time points (peaks and troughs). Auto-correlograms were used to assess the level of noise (refractory period violations) and cross-correlograms between simultaneously recorded units were used to prevent over-clustering (4).

1.3.4.3 Detection of spikes across tetrodes

Due to configuration of the recording array with a high-density of electrode contacts, the spikes from the same LC neuron could be detected on more than one tetrode. In such situations, we first attempted to merge the spike trains across multiple tetrodes. Merging the spike trains potentially originating from the same neuron and detected on multiple tetrodes should reduce false negatives (missing spikes), as it is common for PCA of waveforms to miss some spikes even if they are part of a well isolated cluster. The assumption is that different spikes are missed on different tetrodes, which were subjected to separate PCA's during clustering. Therefore, spikes missed by PCA on one tetrode could be partly filled in by spikes that were detected on other tetrodes, providing that the tetrodes were recording the same single unit. Merging spike trains across tetrodes operated on the principle that, if the spikes from the same neuron are recorded on 3 adjacent tetrodes and the spike waveforms can be classified into 3 well-isolated clusters, then the spike trains can be merged to yield an equally well-isolated unit. Furthermore, merging across spike trains allows units to be tracked if they drift away from one tetrode and become closer to another tetrode. However, merging procedure needs to avoid inclusion of contaminated spikes originating from neighboring cells. Therefore, merged spike trains must be statistically tested for false positives and conservatively discarded. Unit cluster contamination from other units are typically detected by the presence of spikes during the refractory period. Thus, if the merged spike train did not meet criteria for a single unit activity, then we kept the unit with the least noise (spikes during refractory period).

The merging process consisted in the following steps. First, the cross-correlograms were computed at the sampling rate of the recording (0.04 ms bin width) between the spike trains of a cluster isolated from one tetrode (“reference” cluster) and all other clusters isolated from all remaining tetrodes. If the spike trains associated with the two clustered contained spikes from the same unit, then the majority of spikes would have identical timing with the vast majority (>90%) of spikes being coincidental at time 0 (with a few sampling points of error) and the remaining spikes being missed spikes or cluster noise from other units. Prior recordings using high-density linear electrodes have used cross-correlograms to simply discard one of the trains (5); however, we used merging across tetrodes to reduce missed spikes, In the case that the "reference" and "other" spike trains were mostly coincidental spikes, we attempted to merge them using a procedure, as follows. The coincident spikes in the reference spike train were deleted and the remaining reference spikes were merged with the spikes from the other spike train, resulting in a new "merged" spike train. The amount of noise (number of spikes during the

refractory period) and total number of spikes in the train were recorded for the original "reference" spike train, original "other" spike train, and newly merged spike train. A Fisher's Exact Test was performed to statistically assess if the proportion of contaminated spikes added by merging is significantly greater than the proportion of noise (refractory period) spikes in either the original reference spike train or the original other spike train. The Fisher's test was run separately for merged versus reference and the merged versus other spike trains. A result of non-significance (with alpha set to 0.01 and a right-sided test) for *both* the original reference spike train and the original other spike train indicated that the original spike trains do *not* have *greater* odds of having noise than the merged spike train. In this case, the merged train may be kept because the amount of noise was not increased beyond its level in the original two trains. The original spike trains were discarded. However, if the test is significant for either of the original trains, then either the reference spike train or the other spike train is kept depending on which has a lower percentage of spikes during the refractory period out of the total number of spikes. The merged spike train was discarded. The merging procedure was repeated for each cluster from each tetrode until conflicts no longer existed.

1.3.4.4 Assigning unit location on recording array

Isolated single units were assigned a channel location on the electrode array according to which electrode measured the highest mean waveform amplitude (averaged from all spikes). In the case of single units with spikes that were merged across tetrodes (see section 1.2.3.4), a list tracked the tetrodes on which the unit appeared and the location was assigned to the channel with the maximum amplitude when considering all of the tetrodes that recorded the unit.

The spacing between all 32 channels was 25 μm, which allowed us to use Pythagoras' Theorem to calculate a distance between channels on the array. The distance between each unit's maximal waveform amplitude was used to measure the distance dependence of spike count correlations and cross-correlograms.

1.3.5 Sensory stimuli

Sensory stimuli were foot shocks delivered to the contralateral hind paw. Pulses were square, biphasic, and 0.005 msec duration at 5 mA. Pulses were delivered at two frequencies (single pulse or five pulses at 30 Hz). Fifty trials of foot shock stimuli were delivered with an inter-trial interval of 2000±500 msec.

1.3.6 Intra-cranial stimulation

Brain regions were stimulated in a random order. Pulses were square, biphasic, and 0.25 msec duration over a range of intensities (400 - 1200 μA). Pulses were delivered at a range of frequencies (single pulse or 4 pulses at 10 - 80 Hz). The pulse waveforms were constructed in Spike2 (CED) and delivered via a current generator (in-house constructed), which allowed recording of the stimulation voltage at the tip of electrode, which was also digitized and stored and used to verify stimulation. Stimulation was delivered with an inter-trial interval of 2000±500 msec. At least 50 trials of each intensity and frequency were repeated in random order for each brain region.

1.4 Materials and Methods: Pharmacology

1.4.1 Administration of clonidine

At the end of the recording, clonidine was injected intra-peritoneal (i.p.) at ~ 2 min after the start of the final recording session. Clonidine (Sigma-Aldrich, product identification: C7897) was prepared as a 0.5 mg/ml solution in normal saline and stored at room temperature. The solution was injected in a dose of 1.0 mg/kg body weight. The recording was continued at least until all activity, included multi-unit activity, ceased.

1.5 Materials and Methods: Histology

Rats were euthanized with pentobarbital sodium (Narcoren Merial) via an i.p. injection (100 mg/kg). The rats were then trans-cardially perfused with 0.9% saline and then 4% paraformaldehyde (PAF) in 0.1M phosphate buffer (pH 7.4). The brain was removed and stored in 4% PAF. Brains were moved into 30% sucrose, until they sank, before sectioning on a freezing microtome (Microm, model: HM 440E). Coronal sections (50 μm thick) were collected into 0.1M phosphate buffer and directly stained. For sections containing the LC, alternating sections were stained for Nissl substance or the catecholamine synthesis enzyme, tyrosine hydroxylase (TH). Sections containing cortical and sub-cortical regions were stained for Nissl substance. Staining for TH was performed using a 1:500 dilution of monoclonal mouse anti-TH antibody (ImmunoStar) and a 1:400 dilution of biotinylated, rat absorbed anti-mouse secondary antibody (Biozol) in PB. The antibody was visualized using a DAB and horse radish peroxidase reaction with hydrogen peroxide using a standard kit (Biozol, model: Vectastain Elite ABC-Peroxidase Kit CE). After staining for TH or Nissl, sections were mounted on gelatin-coated glass slides, dehydrated in an alcohol series, cleared (Carl Roth, Roti-histol), and cover slipped with DPX slide mounting media (Sigma-Aldrich, catalog number: 06522).

1.6 Materials and Methods: Data Analysis

1.6.1 Spike count correlations

The Pearson's correlation coefficient was used to quantify the correlation between spike counts. Spontaneous spiking excluded the 1 sec period following foot shock stimulation or intra-cranial stimulation. Spontaneous spikes were also excluded during inactive periods in which the rate was less than 0.5 Hz due to quiescence of all single and multi-unit activity in the LC (paradoxical sleep, (2). Spontaneous spike count correlations were then calculated from the time bins (200 msec or 1000 msec) in which both neurons were active. Evoked spike count correlations after foot shocks were calculated from the trial-by-trial spike count in a single window after stimulus onset (50 msec or 200 msec). Spike count correlations before and after prefrontal cortex stimulation were calculated from the trial-by-trial spike counts in a 200 msec window before and after stimulation. Spike counts were Z-scored to remove the influence of the firing rate change evoked by PFC stimulation, so that the spontaneous and evoked activity could be compared (6,7).

1.6.2 Cross-correlograms

We calculated cross-correlograms between spike trains in order to infer the potential connectivity patterns underlying synchrony. We focused our analysis on two connectivity patterns: common synaptic input (network interactions) and gap junctions. Significant changes in coincidental spike count were detected by comparing the observed counts to 1000 surrogate cross-correlograms generated from jitter spike times (8). This approach uses the data to determine the degree of coincident spiking expected by chance and it also excludes synchrony due to interactions at slower time scales than those of interest. Briefly, the spike times for each unit were jittered on a uniform interval and a surrogate cross-correlogram was calculated between the jittered spike times; this process was repeated 1000 times. Significant cross-correlogram bins were those that crossed both a 1% pairwise expected spike count band and a 1% globally expected spike count band (the maximum and minimum counts at any time point in the cross-correlogram and any surrogate cross-correlogram). For network interactions, the cross-correlograms were calculated in a window of 2000 msec, a bin size of 10 msec, and a uniform jitter interval of ±200 msec. Any significant coincidental spiking excludes synchrony due to co-variation of spiking on a timescale of a few hundred milliseconds. For gap junction interactions, we used a window of 3 msec, a bin size of 0.05 msec, and a uniform jitter interval of ±1 msec.

1.6.3 Syn-fire chain analysis

Repeating sequences of triplets and quadruplets of neuronal spiking were measured using three steps: (*i*) a spike-by-spike search, (*ii*) template-formation, and (*iii*) template matching algorithm (9,10). The analysis stepped through all simultaneously recorded units $n \rightarrow N$ and all of the spike times for each unit ($n_{m \rightarrow M}$). The spike search started with the first unit and its first spike, n_m. This spike time was a reference event marking the start of a 2 msec window during which we identified any other spiking units. The sequence of units and the delay between their spikes was stored as a template. For example, n_m might be followed 1.1 msec later by a spike from unit $n = 5$ which is subsequently followed 0.8 msec later by a spike from unit $n = 30$. This forms a template of 1 – 5 – 30 with delays of 1.1 msec and 0.8 msec. The next step, template matching, would proceed through the spikes $1_{m+1 \rightarrow M}$ and attempt to match the template and its delays. A 0.4 msec window of error was allowed around each spike in the original template for matching. Thus, for each spike of unit $n = 1$, unit $n = 5$ could spike between 0.7 msec and 1.5 msec after unit $n = 1$ and unit $n = 30$ could spike 0.4 msec to 1.2 msec after unit $n = 5$. A template match would be counted if the spikes of the other units aligned with the originally formed template. For each template, the total number of observations was compared to the number of observations in the top 1% of 100 surrogate data sets in which spike times were jittered on a uniform interval by 1 msec. Any sequential spike patterns that occurred more often than expected by chance were counted as significantly occurring chains of spikes.

1.6.4 Graph theory analysis and ensemble detection

For each rat, a graph was constructed with each unit as a node. Links were drawn between units with strong spike count correlations, following the methods of Rubinov & Sporns (2010) and Bruno et al. (2015) (11,12). The threshold for drawing a link was set as the highest possible value such that the mean network degree was less than the log(N), where N is the number of nodes in the graph (13). Units without strongly correlated activity were left unlinked. The resulting network was represented by a binary adjacency matrix. We calculated the small-world coefficient as the ratio of the network clustering coefficient to the network path length, so that a coefficient greater than 1 indicated a small-world network topology (13). The small-world coefficient was normalized using a non-parametric permutation of the network. Clustering and path length were normalized by mean values calculated from 1000 surrogate networks with shuffled links, but the number of nodes, links, and degree distribution were preserved. Ensembles were detected by segregating nodes into groups that maximize the number of links within each group and minimizes the number of links between group. The iterative optimization

procedure used a Louvain community detection algorithm to maximize a modularity score (Q) quantifying the degree to which groups separate (12,14). The degree of ensemble separation (Q) was compared to modularity scores from 1000 from shuffled networks. If Q was higher than the top 5% of the 1000 surrogate values, then adequate separation of units into ensembles was achieved. All graph theory and ensemble detection analyses were implemented in MATLAB using the Brain Connectivity Toolbox (15).

1.6.5 Oscillations in spike count

Single unit spike trains were first convolved with a Gaussian kernel with a width of 250 msec and a sampling rate of 1 msec. The resulting spike density functions (SDF) were analyzed for the power of oscillations, the phase of oscillations, and the coherence between pairs of SDF's. The power spectral density of each spike train was calculated using a multi-taper method in MATLAB (Chronux Toolbox, (16)). We used 19 tapers with a time-bandwidth product of 10. The frequency band was 0.01 to 10 Hz. We used finite size correction for low spike counts. Instantaneous phase was extracted by first filtering the SDF with a 3rd order Butterworth filter at a particular frequency of interest (0.09 to 0.11 Hz and 0.40 to 0.48 Hz) and then obtaining phase from the Hilbert transform of the signal. The consistency of the instantaneous phase difference between each unit pair was assessed using Rayleigh's Test for Circular Uniformity ($p<0.05$), which was implemented in MATLAB (Circ_Stat Toolbox, (17)). Coherence between pairs of units was calculated using the Chronux Toolbox in MATLAB with the same parameters used for calculating the power spectral density. Coherence and power were averaged across all single units and smoothed with a width of 0.15 Hz.

1.6.6 Spike-LFP phase locking

Local field potential (LFP) was recorded in the prefrontal cortex. The LFP was lowpass filtered with a 3rd order Butterworth filter at 2 Hz. The instantaneous phase was obtained by Hilbert transformation. Spike times corresponded to LFP phases. For each single unit, the phase distribution was tested for significant locking to cortical LFP using Rayleigh's Test for Circular Uniformity ($p<0.05$).

1.6.7 Antidromic spiking

Forebrain regions were stimulated in a randomized order with single pulses at currents of 400, 600, 800, 1000, and 1200 μA. Stimulation was delivered with a 2 sec inter-trial interval with 500 msec jitter. Peri-stimulus time histograms were Z-scored to 1 sec before stimulus onset. If a single bin (5 msec) Z-score exceeded 5 and no other bins were significant, then the

unit was marked as antidromically activated. Spike rasters of these units were manually inspected.

1.6.8 Orthodromic spiking

The prelimbic (PL) and infralimbic (IL) divisions of the PFC were stimulated across a range of frequencies (10 – 80 Hz) and currents (0.2 mA – 0.8 mA). Units were grouped by K-means clustering of the peri-stimulus time histograms and considered to be responsive units if the mean of their group crossed a Z-score of ±2. A very large K (10) was used to over-cluster the data. This resulted in, for example, one responsive group being divided into more than one responsive group, but unit members of these groups were combined later when generating a list of responsive units. A unit was counted as responsive if it responded at any frequency or current. Latency to respond was determined as the time of maximal change in rate from baseline (1 sec before stimulation) for each individual unit in a responsive group.

1.6.9 Brain state

Cortical state was recorded on cortical electrodes in the PFC. The LFP was divided into 6 sec epochs and the distribution of LFP voltages was obtained for each epoch. The distribution was tested for bimodality using Hartigan's Dip Test ($p<0.05$). A non-significant dip test selected for epochs of LFP that were relatively flat (activated state or mixture of activated and slow oscillations). A significant dip test selected epochs that were bimodal and therefore either very slow oscillations or slow oscillations. We then separated activated states from mixture states by examining the kurtosis of the LFP voltage distribution, with high kurtosis values indicating a sharply peaked distribution with very little variability (activated state). The distribution of kurtosis values was bimodal, which suggested that epochs of LFP clustered into activated or mixed states. We also separated those states with a significant dip test into very slow oscillation states and slow oscillation states using the proportion of the power spectrum of each LFP epoch that was very low frequency (<0.4 Hz). The distribution of power ratios was bimodal, which suggested that epochs of LFP clustered into very slow oscillation and slow oscillation states. Each 6 second epoch of LFP (and its voltage distribution) was thus associated with 3 values: a dip test p value, kurtosis, and power ratio. These values were used with K-means clustering to assign each LFP epoch a state: activated, mixture (activated and oscillations), slow oscillations, very slow oscillations, and unclassified.

1.6.10 General statistics

All results were assessed using ANOVA and then a post-hoc Tukey-Kramer test. If data were not normal, then a Mann-Whitney test was used. For circular data, uniformity was assessed using Rayleigh's Test for Circular Uniformity. Proportions were compared using a chi-squared test or, if any table values were less than 5, then a Fishers' Exact Test was used.

2 Supplementary materials: Discussion of brain state determination

We classified 6 sec epochs of LFP into different states: activated (pink), mixture of activated and slow oscillations (black), slow oscillations (green), and very slow oscillations (red), as well as unclassified states (blue). The process is detailed in the methods section. The following figure provides justification for the method. The first step of the method is to obtain a distribution of LFP voltages for each LFP epoch. An example activated state epoch (pink) and an example slow oscillation state epoch (green) is shown.

The method is based on the assumption that dip test for bimodality can separate data into activated / mixed states and very slow / slow oscillation states. We show that kurtosis can divide activated from mixed states, under the assumption that activated states have higher kurtosis than mixed states. Kurtosis values split into 2 distinct distributions corresponding to active (pink) and mixed (black) states. We further show that power ratio can divide very slow oscillation states from slow oscillation states, under the assumption that very slow oscillations generate a power spectrum with greater low frequency components. Power ratio values indeed split into 2 distinct distributions corresponding to slow (green) and very slow (red) oscillation states. Given that kurtosis and power ratio appear to cluster the data into distinct groups after the data are separated based on the dip test for bimodality, it is reasonable that k-means clustering of these three data points would cluster LFP voltage distributions.

Step 1: Get voltage distributions of 6 sec epochs of LFP

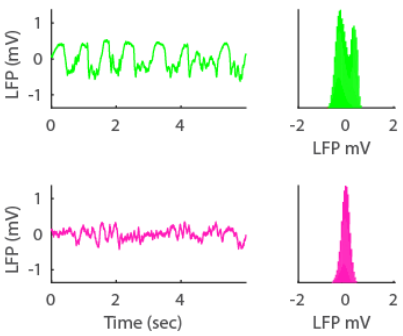

Step 2: Get dip test p value for each voltage distribution

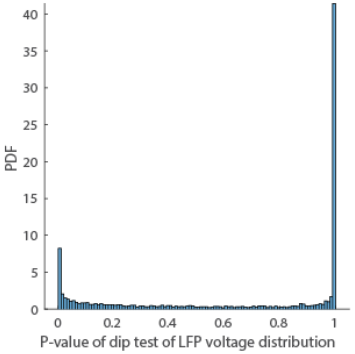

Step 3: Get kurtosis for each voltage distribution

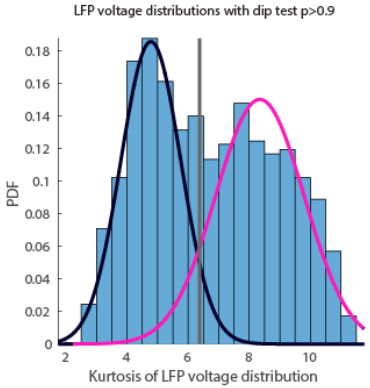

Step 4: Get power ratio for each voltage distribution

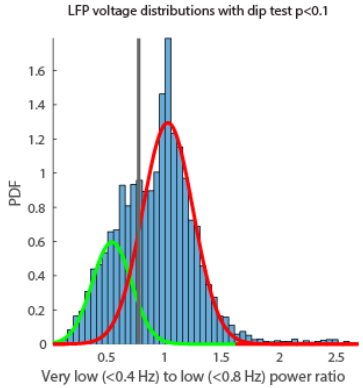

Step 5: Cluster voltage distribution into different states based on dip test, kurtosis, and power ratio

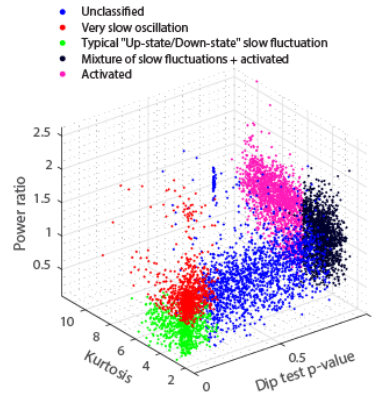

3 Supplementary Materials: Characterization of noradrenergic LC units

Example waveforms and auto-correlograms are shown for a typical experiment (**Supplementary Materials Figure 1A**). Single units exhibited the typical (2,18) low firing rate (0.89 spikes/sec, **Supplementary Materials Figure 2A**) and a characteristic bi-phasic response (excitation followed by inhibition) to sensory stimuli (**Supplementary Figure 2B**). The neurochemical nature of LC units was identified by the presence of auto-inhibitory alpha-2 adrenergic receptors; the alpha-2 agonist, clonidine, inhibited all LC units (**Supplementary Figure 2C**). Therefore, our recordings were confined exclusively to LC-NE neurons.

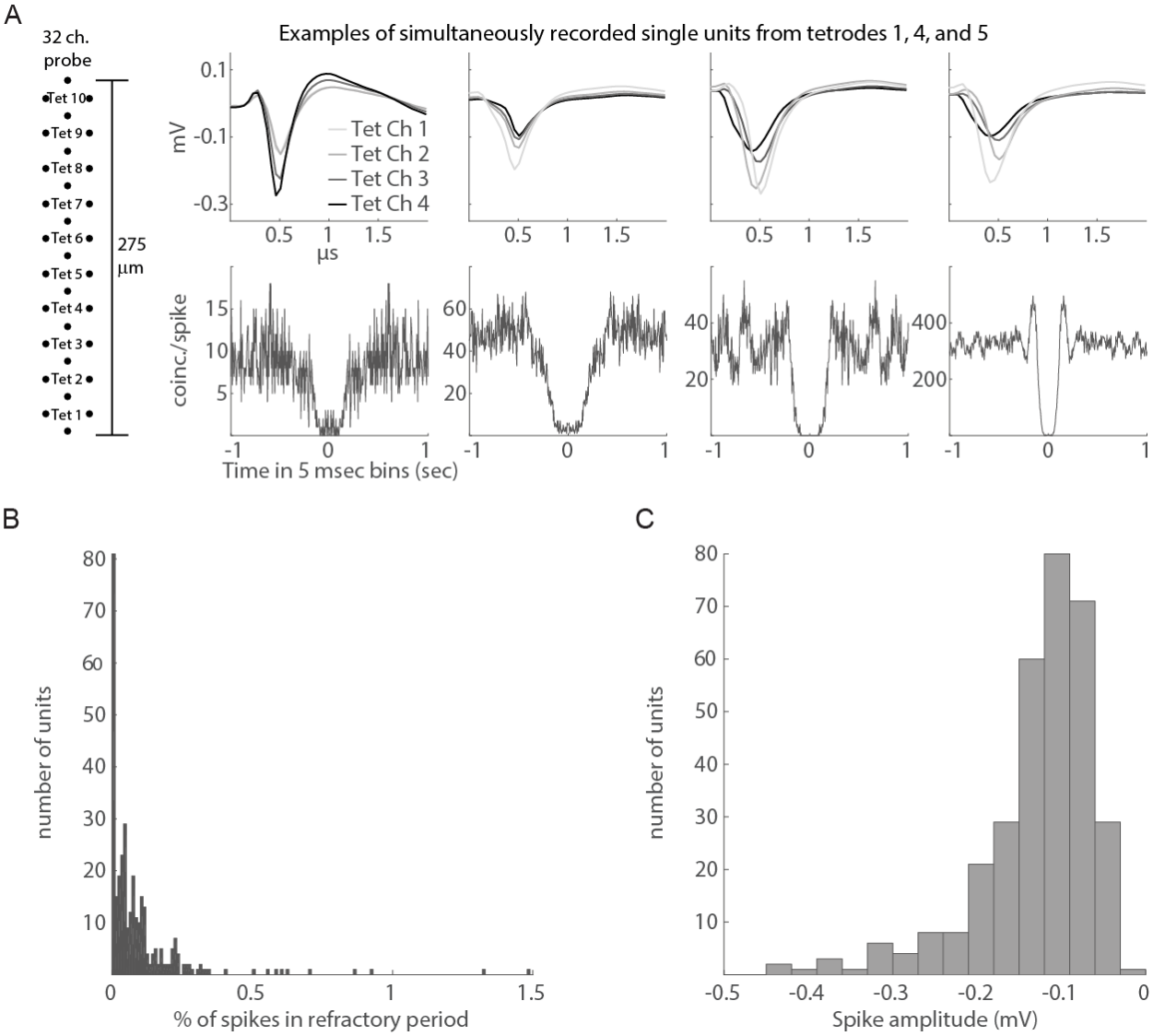

Supplementary Materials Figure 1.

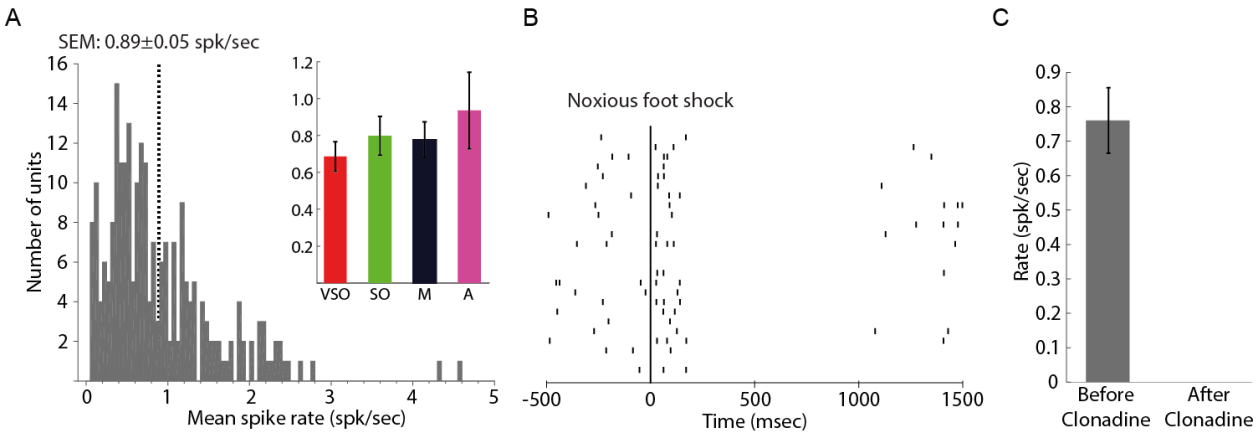

Supplementary Materials Figure 2.

4 Supplemental Materials: References

1. Quiroga RQ, Nadasdy Z, Ben-Shaul Y. Unsupervised spike detection and sorting with wavelets and superparamagnetic clustering. Neural Comput. 2004 Jul 2;16(8):1661–1687.
2. Aston-Jones G, Bloom FE. Activity of norepinephrine-containing locus coeruleus neurons in behaving rats anticipates fluctuations in the sleep-waking cycle. J Neurosci. 1981 Aug;1(8):876–886.
3. Sara SJ, Segal M. Plasticity of sensory responses of locus coeruleus neurons in the behaving rat: implications for cognition. Prog Brain Res. 1991;.
4. Henze DA, Borhegyi Z, Csicsvari J, Mamiya A, Harris KD, Buzsaki G. Intracellular features predicted by extracellular recordings in the hippocampus in vivo. Journal of Neurophysiology. 2000 Jul;84(1):390–400.
5. Erisken S, Vaiceliunaite A, Jurjut O, Fiorini M, Katzner S, Busse L. Effects of locomotion extend throughout the mouse early visual system. Curr Biol. 2014 Dec 15;24(24):2899–2907.
6. Ecker AS, Berens P, Keliris GA, Bethge M, Logothetis NK, Tolias AS. Decorrelated neuronal firing in cortical microcircuits. Science. 2010 Jan 29;327(5965):584–587.
7. Bair W, Zohary E, Newsome WT. Correlated firing in macaque visual area MT: time scales and relationship to behavior. Journal of Neuroscience. 2001 Mar 1;21(5):1676–1697.
8. Fujisawa S, Amarasingham A, Harrison MT, Buzsáki G. Behavior-dependent short-term assembly dynamics in the medial prefrontal cortex. Nat Neurosci. 2008 Jul;11(7):823–833.
9. Luongo FJ, Zimmerman CA, Horn ME, Sohal VS. Correlations between prefrontal neurons form a small-world network that optimizes the generation of multineuron sequences of activity. Journal of Neurophysiology. American Physiological Society; 2016 May 1;115(5):2359–2375.
10. Ikegaya Y, Aaron G, Cossart R, Aronov D, Lampl I, Ferster D, et al. Synfire chains and cortical songs: temporal modules of cortical activity. Science. American Association for the Advancement of Science; 2004 Apr 23;304(5670):559–564.
11. Bruno AM, Frost WN, Humphries MD. Modular deconstruction reveals the dynamical and physical building blocks of a locomotion motor program. Neuron. 2015 Apr 8;86(1):304–318.
12. Rubinov M, Sporns O. Complex network measures of brain connectivity: uses and interpretations. NeuroImage. 2010 Sep;52(3):1059–1069.

13. Watts DJ, Strogatz SH. Collective dynamics of “small-world” networks. Nature. 1998 Jun 4;393(6684):440–442.
14. Blondel, et al., Fast unfolding of communities in large networks. Journal of statistical …. 2008 Oct 1;2008(10):P10008.
15. Bullmore E, Sporns O. Complex brain networks: graph theoretical analysis of structural and functional systems. Nat Rev Neurosci. 2009 Mar;10(3):186–198.
16. Mitra P. Observed Brain Dynamics. Oxford University Press; 2007. 1 p.
17. Berens P. CircStat: a MATLAB toolbox for circular statistics. Journal of Statistical Software. 2009;.
18. Aston-Jones G, Bloom FE. Norepinephrine-containing locus coeruleus neurons in behaving rats exhibit pronounced responses to non-noxious environmental stimuli. J Neurosci. 1981 Aug;1(8):887–900.